RADIATION SOURCE DETECTION FROM MOBILE SENSOR NETWORKS USING PRINCIPAL COMPONENT ANALYSIS

BY

JIFU ZHAO

THESIS

Submitted in partial fulfillment of the requirements
for the degree of Master of Science in Nuclear, Plasma and Radiological Engineering
in the Graduate College of the
University of Illinois at Urbana-Champaign, 2016

Urbana, Illinois

Master's Committee:

Assistant Professor Clair J. Sullivan, Advisor
Assistant Professor Zahra Mohaghegh

Abstract

Detecting the presence of possible illicit radioactive materials in large areas is challenging because of changing background radiation, shielding effects and short collection time, especially when the radioactive materials are moving. The concept of mobile sensor networks is put forward to solve this problem. In this thesis, a small mobile sensor network is established using commercially available radiation detectors and cell phones. A spectrum decomposition and reconstruction method based on Principal Component Analysis (PCA) is proposed to work with mobile sensor networks. Two experiments are designed to test this method's performance on real-world data. The PCA-based method's performance is analyzed using receiver operating characteristic, or ROC curves. Further study finds that although the PCA-based method doesn't work well on current mobile sensor networks, its performance can be improved by increasing the radiation spectral quality.

Acknowledgments

First and foremost, I would like to thank my parents and Chunyan Hao for their endless love and support on my road to knowledge.

I would like to express my sincere thanks to my advisor, Professor Clair Sullivan. This work would not have been possible without her support and guidance.

In addition, I want to express my thanks to Professor Zahra Mohaghegh and Professor James Stubbins for investing time and efforts to help me improve this thesis.

Finally, I want to thank my group members for their instructive discussions and for their kind helps in the past two years.

Table of Contents

List of Tables

List of Figures

Chapter 1

Introduction

1.1 Radiation Detection Problems

Radiation detection is crucial to the nation's security. Nuclear weapons or radiological dispersal devices are big threats to the nation's security. There is a need to effectively and accurately detect special nuclear materials (SNM). Currently, detector systems positioned at key choke points such as airports or customs, have been deployed to prevent the entry or exit of radioactive sources. However, only preventing the entry or exit of these materials is not enough. Some materials that are already in the country, such as the sources for medical or research purposes, can also be used by terrorists. In this case, a monitoring system that can be distributed in large areas, like cities, and can detect moving sources is needed to ensure the nation's security.

There are many challenges in the radiation detection field. One big challenge is the background radiation. Background radiation always exists and it can be dramatically influenced by weather conditions, the surrounding environment and so on. As the distance becomes larger, the signal from actual sources becomes weaker as a function of $1/r^2$. The noise, which comes from background radiation, will remain almost the same or even stronger. In this case, it becomes much harder to correctly detect, locate, and identify the potential sources. Another challenge is the impact of shielding. The shielding materials reduce the signal strength and make it difficult to detect. The last main challenge is time. Radioactive materials can be transported via vehicles and may be used at any moment. It is important to quickly determine the existence of radioactive sources. So, in summary, a successful radiation monitoring system should have the following capacities:

1. **Sensitivity:** It should have enough sensitivity to detect not only the strong radioactive sources, but also the weak sources. This relies on the development of new generation of detectors.

2. **Accuracy:** High false alarm rates can cause a severe waste of resources. A successful system should have a high true positive rate while keeping a low false positive rate.

3. **Adaptability:** Weather conditions and the surrounding environment are always changing with time and location. A good system should be able to work under different conditions. In addition, it shouldn't only work for stationary sources, but also for moving sources.

4. **Efficiency:** As mentioned, time is a big challenge for radiation detection. A good system should be able to detect, locate and identify all possible sources in a limited time period, especially for moving sources. This implies both the need for highly-efficient detectors as well as computationally-efficient analysis algorithms.

To develop a radiation detection system that satisfies these four requirements, not only the new generation of detectors that have high resolution, high efficiency and good mobility, but also the new algorithms to efficiently process the data and make the right decisions are needed. This thesis focuses on developing appropriate algorithms to fulfill these requirements.

1.2 Background Radiation

Background radiation refers to the naturally existing radiation. All humans are continuously exposed to these kinds of radiation. Natural radiation sources include [1, 2]:

1. **Cosmic rays** that come from outer space and from the surface of the Sun.

2. **Terrestrial radionuclides** that occur within the Earth's crust, in building materials, air, water, foods and in the human body itself. They mainly come from ^{40}K and the daughter products of the decay series of ^{238}U, ^{232}Th, ^{226}Ra and ^{235}U [3].

Background radiation amost never remains the same. It can fluctuate with time, weather conditions, surrounding environment, and so on. It has been proven that during periods of precipitation, the background radiation level will increase [4, 5]. In addition, soil conditions are found to affect the background radiation level [6]. Some of theses variations are easy to explain based on the surrounding environments. The changing background radiation is the main challenge for detecting the movement of small sources.

1.3 Radiation Detection Algorithms

Under the changing background radiation conditions, and with the impact of shielding, the signals that come from actual sources are hard to distinguish, especially when the background radiation level is high and the distance to the source is large. In other words, the real-world radiation data will be very noisy and

the signal-to-noise ratio will not be high. Developing appropriate methods to extract useful information from the noisy signals is needed. Researchers have been working together to develop appropriate radiation detection algorithms. According to the number of used detectors, these algorithms can be categorized into two types: single detector-based algorithms and sensor network algorithms. In this section, a brief overview of different algorithms in radiation detection is given.

1.3.1 Single Detector-Based Algorithms

Single detector-based systems have been developed for a long time. Traditionally, there are two methods of detection: active and passive detection [7]. In active detection, the materials of interest are exposed to neutrons or high-energy photons. The gamma rays associated with fission products are then measured. Additionally, neutron detectors are employed to measure increases in neutron counts that is indicative of fission. Special nuclear materials can be determined upon analyzing the spectra [8, 9]. Active detection can be used in airports or customs, but it is expensive and lacks mobility. This makes it unsuitable for large scale detection, especially when there are moving sources. On the other hand, passive detection doesn't need to generate neutrons or photons and measures the emitted radiation directly. Passive detection is widely used in radiation detection fields. The existing algorithms, which either analyze the gross count rate or the spectra, are almost based on passive detection. These algorithms can be categorized into the following three types:

1. **Gross Count Rate:** This method uses count rate information only. In this method, a predetermined threshold is used to determine whether or not there are sources. If the collected data are above the threshold, it is assumed that some possible source has been detected [10, 11]. Usually, the threshold is set to be k times of the standard deviation of the estimated background count rate. So this method is also called the k-sigma method. The k-sigma method is a very direct and simple method, but it can produce high false alarm rates.

2. **Spectrum Fitting:** This method uses the spectral information instead of count rate information. It fits the measured spectrum with different templates from pre-calculated library [11]. Spectrum fitting methods can work well when the spectra are well-collected, but when the collection time is short and the spectral quality is not high, its performance will be affected.

3. **Machine Learning:** This method contains different algorithms that mainly focus on spectral information. In this method, a classifier is trained through different algorithms, such as Support Vector Machine (SVM) and Random Forests [11]. Then the trained classifier is used to classify new spectra

into threat or non-threat categories. This method needs a lot of pre-labelled data to train the classifier. It works well for the cases that only particular sources are included. However, when there are unknown sources or the background radiation is changing, correctly labelling the training data are almost impossible.

1.3.2 Sensor Network Algorithms

Single detector systems are suitable for stationary sources in a small area. When the sources are moving and the area of interest is large, single detector systems are no longer suitable. In this case, networked arrays of sensors are beneficial. Sensor network detection systems refer to the systems that use multiple detectors to detect and locate either stationary or mobile sources. With multiple detectors, new methods are needed to extract useful information from multiple detectors and give more robust conclusions. Several methods have been developed to improve sensor network detection systems' performance.

1. **Bayesian Methods:** Bayesian algorithms compute the posteriori probability distribution based on an estimated prior distribution [12]. It has been proven to have some good results on certain simulated scenarios [13–16]. However, its results are based on the prior estimates, which are hard to accurately determine, especially when the background radiation cannot be simply modeled by Poisson processes [12].

2. **Maximum Likelihood Estimation(MLE):** MLE is a widely used method for parameter estimation. The MLE method has been successfully used to estimate the source parameters and source numbers [17]. However, MLE has been proven unsuitable for scenarios where there are more than three sources [17]. In addition, MLE requires extensive computations [12], which makes it unsuitable for real-time radiation detection.

3. **Sequential Probability Ratio Test(SPRT):** SPRT is a widely used hypothesis testing method. It compares current measurements to previous baseline [11]. SPRT is useful for long-term radiation monitoring [18] and for low-level point source detection and localization with stationary detectors [19, 20].

Besides the above methods, there are also other methods being developed to address the similar problems, such as Mean of Estimates [21], Least Squares Estimation [22] and Interactive Pruning [23]. These methods show some improvement over other methods, but their results are mainly based on simulations and their performance on real-world data need to be tested.

1.4 Mobile Sensor Networks

Sensor network detection systems that use stationary detectors have some advantages over single detectors, even when the detectors' sensitivity or resolution are not as good as single detectors. It has been proven that distributed detector systems have improved performance over a single detector [24]. Chandy et al. found that the networks of static sensors can help people rapidly locate the radiation sources [14]. Nemzed et al. noticed that with an array of detectors, the signal-to-noise ratio (SNR) increased along a $\sqrt{N}$ curve for small numbers of detectors [16].

However, with a fixed number of detectors, the area that can be covered is predetermined. People have studied the optimal number of detectors needed in a pre-defined area through simulations [14]. When the search area is large, like a big city, the cost for detectors would be prohibitive. To solve this problem, the concept of a mobile sensor network has been put forward.

Mobile sensor networks are easily deployable. Since each detector in mobile sensor network is usually small, it uses less energy per detector. More importantly, all detectors are mobile. With the same amount of detectors, mobile sensor networks can cover larger areas than stationary sensor networks. Studies have shown that mobile sensor networks are more effective than stationary sensor networks [14].

Mobility is one of mobile sensor networks' biggest advantage. However, mobility also brings some problems. For some traditional methods, such as Maximum Likelihood Estimation and Least Square Estimation, the location of radioactive source is determined according to the data acquired from surrounding detectors. However, in mobile sensor networks, detectors are always moving and the source may not be surrounded by any detectors. These methods cannot be directly applied without modification. New methods need to be developed. Research has been done to solve similar problems. For example, Hochbaum et al. used network flow method to simulate the scenario of locating illicit radioactive sources in an urban environment [25, 26]. Tandon et al. used a Bayesian aggregation method to locate and infer properties of radioactive sources through mobile sensor networks [27].

Although a promising radiation detection method, there are still a lot of problems to be solved for mobile sensor networks. This thesis manly focus on studying the performance of spectral decomposition and reconstruction method based on Principal Component Analysis to analyze the data acquired through mobile sensor networks.

1.5 Chapter Review

There are five chapters in this thesis. Chapter 1 describes the radiation detection problems and then gives an overview of existing algorithms for single and multiple detector systems. Chapter 2 focuses on the technical background of Principal Component Analysis (PCA) and the corresponding spectrum reconstruction principles. Chapter 3 describes the detector systems used in this thesis and the experiment design. Chapter 4 analyzes the results and gives some explanations. Finally, a short summary and an outlook of possible future work are given in Chapter 5.

Chapter 2

Technical Background

With the development of new generation detectors, not only the count rate information, but also the real-time spectral information can be collected. However, the shielding effects and the distance from the radioactive sources weaken the signal strength. Additionally, the changing background radiation increases the noise level. All these factors reduce the signal-to-noise ratio (SNR) and make it difficult to detect the source with low false alarm rates.

To effectively solve this problem, one direct idea is to separate the background radiation from the observed spectra. If the background radiation can be successfully separated, the rest can be used to determine the existence of possible sources. In this way, radiation detection becomes very simple and direct. However, the background radiation keeps changing all the time and it is very hard to accurately separate it.

In this chapter, a review of existing background radiation estimation methods is given at first, then a spectral decomposition and reconstruction method based on Principal Component Analysis (PCA) is proposed. Finally, some simple examples are given to help understand this method.

2.1 Background Radiation Estimation

As mentioned in chapter 1, background radiation exists everywhere. It can change with time, surrounding environment, weather conditions and so on. For a large area, it is almost impossible to constantly and accurately measure the background radiation. The random nature of background radiation and the lack of prior information makes it necessary to develop some dynamic methods to efficiently estimate the background radiation under different conditions [28].

Currently, several methods have been developed to estimate and separate the background radiation. Kirkpatrick et al. used Poisson statistics to compute the background contributions to gamma spectra, which proved to be a sensitive method for the detection of small signals in low-count spectra [29]. Through making the assumption that the background varied smoothly while the signal varied more rapidly, Fischer et al. proposed the Bayesian method to estimate the background radiation spectra [30]. A statistics-sensitive

non-linear iterative peak-clipping (SNIP) based method was applied on γ-ray spectra to determine the peak regions and then eliminated the background in the spectra [31,32]. An iterative filtering method was proposed by Zhu et al. to estimate the background in noisy spectroscopic data [33]. Based on the assumption that the local minimum belonged to the background radiation, Alamaniotis et al. proposed kernel-based machine learning method to estimate the background radiation for low-count gamma-ray spectra with unknown sources without any prior information [28]. The estimated background spectra from this method had the right shape, but the amplitude of the estimated background spectra was either too high or too low. An algorithm that coupled robust Kalman filter and EM framework was designed by Fraschini and Chaillan to recursively estimate the background spectra [34]. In addition, other methods, such as spectral peak erosion [35], digital filters, and Monte Carlo simulations [36] are also used to estimate the background radiation.

However, among the proposed methods, a few need to manually evaluate some parameters as the prior information, some methods require long computation time, while other methods focus on high-resolution spectra [28]. For mobile sensor networks, the data will be constantly collected for one to two seconds only. This means that the spectra will be low-count and low-resolution. Dynamic methods are needed to estimate the background radiation for low-count and low-resolution spectra of unknown sources. In this thesis, a PCA-based spectral decomposition and reconstruction method is proposed to estimate the background radiation under varying conditions.

2.2 Principal Component Analysis

Principal Component Analysis (PCA), also known as Karhunen-Loève transform [37], is a widely used method for feature generation and dimensionality reduction. PCA uses an orthogonal transformation to convert a set of possibly-correlated variables into a set of linearly-uncorrelated variables called principal components. The number of principal components will be less than or equal to the number of original features (dimensions). For convenience, all principal components are sorted according to the variance that is explained by each principal component. In this way, the first principal component can explain the largest variance among all components. The second component is uncorrelated (orthogonal) to the first component and can explain the second largest variance and so on for the succeeding components. The original data can then be represented by the principal components in a new space.

To better understand this process, some derivations are shown as follows. In general case, assume every input data is an m dimensional row vector:

$$\vec{x_i} = [x_i^1, x_i^2, \cdots\cdots, x_i^m] \tag{2.1}$$

where m is the number of features. If there are n sample data in total, then the dimension of given data will be n by m.

$$X_{n\times m} = \begin{bmatrix} \vec{x_1} \\ \vec{x_2} \\ \vdots \\ \vec{x_n} \end{bmatrix} = \begin{bmatrix} x_1^1 & x_1^2 & \cdots & x_1^m \\ x_2^1 & x_2^2 & \cdots & x_2^m \\ \vdots & \vdots & \ddots & \vdots \\ x_n^1 & x_n^2 & \cdots & x_n^m \end{bmatrix}_{n\times m} \tag{2.2}$$

Usually, the first step of PCA is to standardize the data. In this thesis, since the spectra have the same unit for each channel, this process can be simply done by subtracting the mean value for each channel. The mean value, which corresponds to the average background radiation, can be calculated as follows:

$$mean_j = \frac{1}{n}\sum_{i=1}^{n} x_i^j \tag{2.3}$$

where $mean_j$ is the mean value of jth dimension of all background radiation data.

The mean value vector $\vec{mean}$ is a row vector with m dimensions. So the mean value matrix M can be calculate by multiply $\vec{mean}$ by an n-dimension column vector with all value equals to 1.

$$M_{n\times m} = [1, 1, \cdots, 1]^T * \vec{mean} \tag{2.4}$$

where $M_{n\times m}$ has the same value for each column.

In this way, the centered data $X^c_{n\times m}$, is calculated by:

$$X^c_{n\times m} = X_{n\times m} - M_{n\times m} \tag{2.5}$$

where $X^c_{n\times m}$ has zero mean for each column.

The final goal of PCA decomposition is to find the eigenvectors and eigenvalues for $(X^c)^T * X^c$ [38]. Now, consider the singular value decomposition (SVD) of X^c.

$$X^c = U * \Sigma * V^T \tag{2.6}$$

where Σ is an n by m rectangular diagonal matrix, and its diagonal values are called the singular values of

X^c. U is an n by n matrix, the columns of which are called the left singular vectors of X^c. V is an m by m matrix, the columns of which are called the right singular vectors of X^c. Each column of V is an orthogonal unit vector of length m. In this way,

$$(X^c)^T * X^c = (U * \Sigma * V^T)^T \cdot (U * \Sigma * V^T) \tag{2.7}$$

$$(X^c)^T * X^c = V * \Sigma^2 * V^T \tag{2.8}$$

The columns of V, which are the right singular vectors of X^c, correspond to the eigenvectors of $(X^c)^T * X^c$, and the singular values in Σ are equal to the square roots of the eigenvalues of $(X^c)^T * X^c$. In this way, the original data X^c can be decomposed into a series of eigenvectors.

Since each eigenvector corresponds to a unique eigenvalue, all eigenvectors can be sorted according to the values of eigenvalues in a decreasing sequence. So the first eigenvector corresponds to the largest eigenvalue, which means that the first eigenvector can explain the most variance of the whole dataset. Up to m eigenvectors can be chosen to represent the original data in new space. For example, for any input data $\vec{x_i^c}$ (c implies that the data has been centered), choosing k eigenvectors, after the transformation, the original data becomes:

$$\vec{y_i} = \vec{x_i^c} * V_{m \times k} \tag{2.9}$$

where $V_{m \times k} = (\vec{v_1}, \vec{v_2}, \cdots, \vec{v_k})$ means that only the first k columns of V are chosen.

In summary, the general procedure for PCA decomposition is as follows:

1, Given any n by m input data $X_{n \times m}$, compute the mean values for each dimension, then get the centered input data X^c.

2, Do SVD on X^c, and get the U, V and Σ^2 of X^c.

3, Sort eigenvectors in V according to the eigenvalues from Σ^2 in decreasing sequence.

4, Choose the first k eigenvectors $(\vec{v_1}, \vec{v_2}, \cdots, \vec{v_k})$ from V to transform the original data X^c into new space.

Through the above four steps, the original m dimensional data can be represented through k eigenvectors, which means that the original m dimensional data has been successfully decreased to k dimensions. Since the eigenvectors have been sorted, this transformation can keep as much information as possible.

To show this process clearly, a 2D sample data are chosen as an example. The original data are shown in the first figure of Figure 2.1. The data are represented using two coordinates (X and Y). However, the direction that contains the most variance is neither X nor Y. After PCA, two eigenvectors (red arrows in the second figure) that can represent the variance more clearly are found, which are the first and second principal components. In this way, the original data can be transformed into the new space, which is shown in the third figure in Figure 2.1. After transformation, the original data are distributed with a broader dispersion on the first component direction than the second component direction. In this way, most of its distribution information is kept in the first component direction. Omitting its distribution on the second component direction will not lose much information.

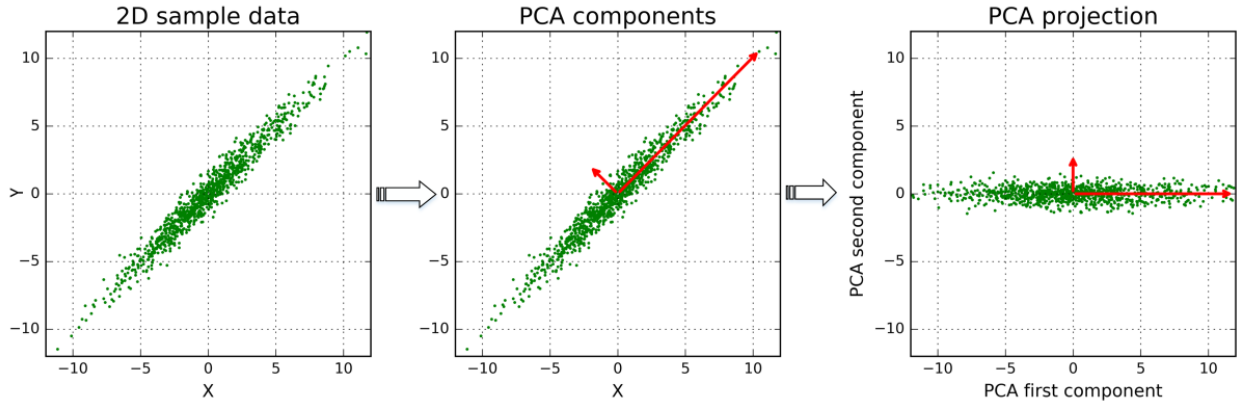

Figure 2.1: PCA decomposition and transformation for 2D sample data

2.3 Spectrum Reconstruction

Through PCA decomposition, a series of eigenvectors $\vec{v_1}$, $\vec{v_2}$, $\cdots$, $\vec{v_m}$ and the average background radiation spectrum $\vec{mean}$ are calculated. New data can be transformed on these eigenvectors. Based on this idea, Runkle et al. transformed observed radiation spectra onto eigenvectors and used the Mahalanobis distance (MD) to perform anomaly detection [39]. This method shows some promising results. However, considering the fact that the spectra from mobile sensor networks are low-quality, this method is not a good choice. In this thesis, a PCA-based spectrum reconstruction method is proposed, which is different from the above PCA/MD method.

Suppose the PCA model is trained based on n background spectra, each of which is an m dimensional row vector, which corresponds to the spectrum with m channels. After PCA decomposition, up to m eigenvectors are obtained, each of which is an m dimensional column vector. All these eigenvectors can be represented

by a matrix with dimension m by m.

$$V_{m\times m} = (\vec{v_1}, \vec{v_2}, \cdots, \vec{v_m}) \tag{2.10}$$

Now, suppose there is an unknown spectrum $\vec{x_i}$, which is a row vector with dimension m. First, the average spectrum $\vec{mean}$ is subtracted from the $\vec{x_i}$ and the centered spectrum $\vec{x_i^c}$ is obtained. Then, $\vec{x_i^c}$ can be represented in new space through projecting $\vec{x_i^c}$ onto the first k eigenvectors.

$$\vec{p_i} = \vec{x_i^c} * (\vec{v_1}, \vec{v_2}, \cdots, \vec{v_k}) = \vec{x_i^c} * V_{m\times k} \qquad k \leq m \tag{2.11}$$

In this way, the original spectrum $\vec{x_i^c}$ will become a row vector $\vec{p_i}$ with dimension k. In order to reconstruct the original spectrum, $\vec{p_i}$ is multiplied by ${V_{m\times k}}^T$, and the reconstructed spectrum $\vec{y_i}$ is obtained:

$$\vec{y_i} = \vec{p_i} * {V_{m,k}}^T + \vec{mean} = \vec{x_i^c} * V_{m\times k} * {V_{m\times k}}^T + \vec{mean} \tag{2.12}$$

Note that when $k = m$,

$${V_{m\times m} * V_{m\times m}}^T = I = {V_{m\times m}}^T * V_{m\times m} \tag{2.13}$$

So, when $k = m$,

$$\vec{y_i} = \vec{x_i} \tag{2.14}$$

This means that, if all the eigenvectors are used to reconstruct the data, no information will be lost. The data are just rotated in the original high dimension space. Apparently, using all eigenvectors cannot help to estimate the background radiation. But what if only part of the eigenvectors are used?

The normal background radiation spectra, which were measured when there were no sources present, could be used to build the PCA model. Since the PCA model is built based on a series of normal background radiation spectra, if only part of the eigenvectors are used to reconstruct the unknown spectra, there is a higher chance of keeping only the background radiation information, while eliminating the unknown source radiation information. Based on this idea, after PCA decomposition and spectrum reconstruction, the difference between original spectrum and reconstructed spectrum will mostly contain the unknown source radiation information. This process can be expressed as follows:

$$\vec{b_i} = (\vec{x_i} - \vec{mean}) * V_{m\times k} * {V_{m\times k}}^T + \vec{mean} \tag{2.15}$$

$$\vec{s_i} = \vec{x_i} - \vec{b_i} \tag{2.16}$$

where $\vec{b_i}$ is the reconstructed spectrum, which is an estimation of background radiation. $\vec{s_i}$ is thought to be an estimation for the unknown source spectrum.

However, after PCA decomposition and reconstruction, some value of reconstructed spectrum $\vec{b_i}$ can be larger than the original spectrum $\vec{x_i}$ or to be negative. Since $\vec{b_i}$ is thought to be an estimate of the local background spectrum, its value should be processed to make sure that they are non-negative as well as smaller than the original spectrum $\vec{x_i}$. In this way, the source spectrum $\vec{s_i}$ will always be non-negative.

The number of eigenvectors, k, can be determined according to different criteria for different purpose. In this thesis, k is determined by choosing the desired variance. For example, if 90% of the total information are to keep, the k is determined to correspond to 90% of the total variance.

To show this process clearly, an example is shown in Figure 2.2. The data included the background radiation spectra as well as the spectra of ^{137}Cs, ^{60}Co and ^{152}Eu. All spectra were collected for 30 seconds using a 2×2 inch NaI detector in laboratory. After PCA decomposition, the first 52 principal components were used to reconstruct the spectra, which corresponded to 60% of total variance. The reconstructed spectra were estimates of background radiation, and the source radiation was separated from the original spectra.

From Figure 2.2, the peak regions for ^{137}Cs and ^{60}Co are easy to find. For ^{152}Eu, since its spectrum is more complex than ^{137}Cs and ^{60}Co, it is a little more difficult to accurately find these peak regions. This will not affect the proposed method's effect.

In conclusion, the proposed PCA-based decomposition and reconstruction method has some theoretical advantages over other methods such as MLE and Bayesian methods:

1, The PCA-based method doesn't require significant computational resources.

2, The PCA-based method is suitable for real-time monitoring. For mobile sensor networks, the spectra are collected every one or two seconds. Real-time detection is needed. This method can fulfill this requirement.

3, The PCA-based method doesn't require many assumptions or prior information. The only requirement is to collect enough normal background radiation data to build the PCA model.

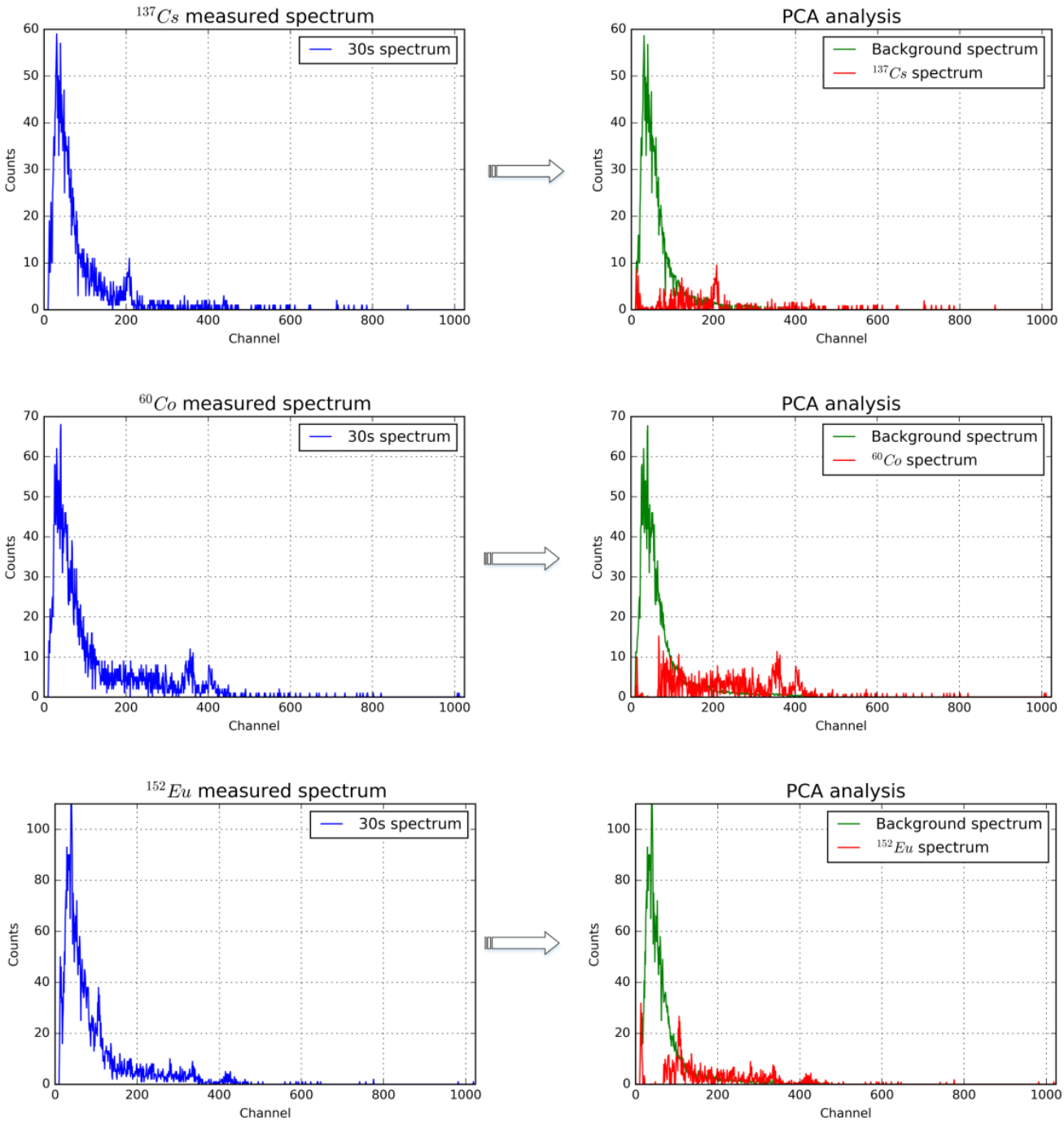

Figure 2.2: Spectrum reconstruction examples (spectra were collected using 2×2 inches NaI detector in laboratory for 30s, and first 52 eigenvectors were chosen to maintain 60% of the total variance)

Chapter 3

Experiment

In chapter 2, some brief deviations were given as the theoretical support for PCA-based decomposition and reconstruction method. It showed some advantages over other methods. To study the performance of the PCA-based method, two groups of data are needed. The first group is the normal background radiation data. This group of data is used to perform PCA decomposition and calculate the eigenvectors. The second group of data, which comes from unknown sources, is used to test this method's performance. In this chapter, the detector systems that were used to build the mobile sensor networks and collect data are first introduced. Then, two experiments that were designed to test the performance of the PCA-based method are described in details. Finally, the ROC curve and the area under the ROC curve, or AUC as a tool to quantitatively measure the system's performance are introduced.

3.1 Detector System Introduction

To satisfy the requirements of ease of mobility, each detector couldn't be too big or too heavy, and it should be able to work wirelessly. In this thesis, the D3S, or Discreet Dual Detectors, from Kromek Group plc. were chosen to build the mobile sensor network. The D3S was a compact wireless, gamma-neutron detector. This thesis only focused on the gamma-ray. For gamma-ray detection, a 2" $\times$ 1" $\times$ 0.5" CsI(Tl) detector was used. The D3S not only collected the gamma ray count rate information, but also the gamma-ray spectral information. The collected spectrum contained 512 channels and the energy range was from $30keV$ to $3MeV$. The detectors collected data for every second and then transferred the data wirelessly to any device that was connected to the detector through Bluetooth. The built-in battery could last up to 12 hours. All these features made it suitable to build mobile sensor networks. For mobile sensor networks, each sensor's real-time location was important. For this purpose, the Samsung Galaxy S6 cell phone was chosen to work together with each D3S detector. In this way, not only the radiation data, but also the GPS data were collected by the phone. A single detector and a coupled cell phone were shown in Figure 3.1.

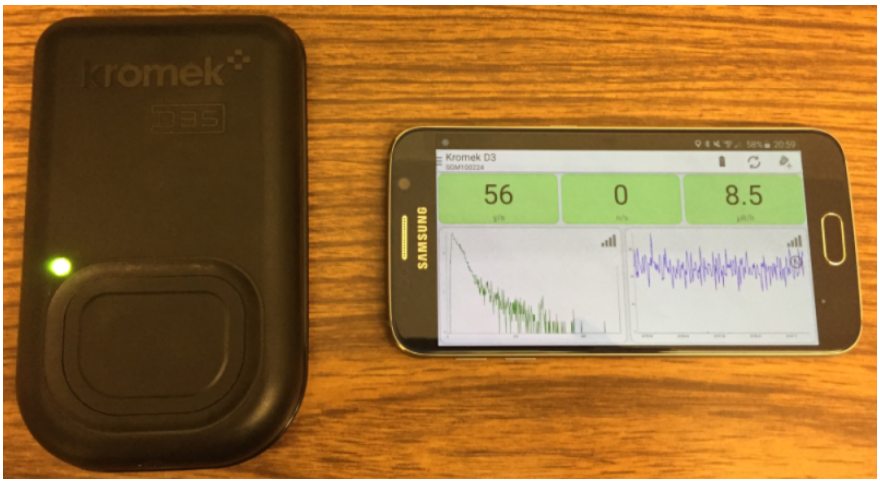

Figure 3.1: Single detector system (the D3S detector and cell phone)

The measured D3S detector intrinsic peak efficiency curve is shown in Figure 3.2. The intrinsic peak efficiency [2] ϵ is calculated by:

$$\epsilon = \frac{Number\ of\ counted\ photons}{Number\ of\ photons\ entered\ to\ detector} \tag{3.1}$$

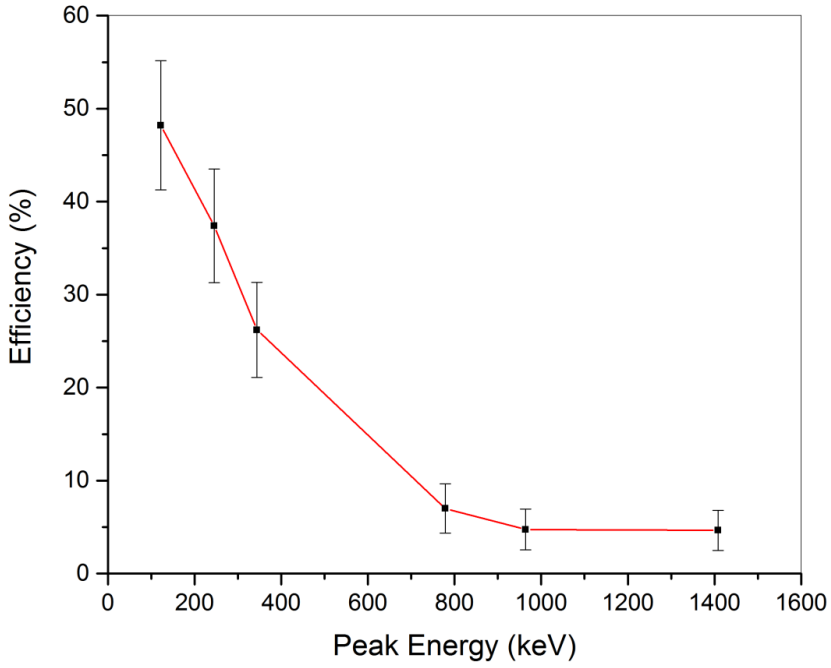

Figure 3.2: D3S detector intrinsic peak efficiency curve (the data were collected through ^{152}Eu for 1 hour)

3.2 Experiment Description

To study the performance of the PCA-based method on real-world data, two experiments were designed. In both experiments, the detectors and phones were carried by different operators. The operators walked steadily and didn't enter any buildings during the experiments. Each experiment collected the normal background radiation data first. Then, with some sources placed at fixed points, this process was repeated again to collect data associated with sources.

3.2.1 Experiment 1

Experiment 1 was designed to test the PCA-based method's overall performance. In this experiment, the engineering campus of University of Illinois at Urbana-Champaign was chosen as the experimental area. The experimental area included some parking lots, buildings and laboratories. A map from Google Earth for this area was shown in Figure 3.3.

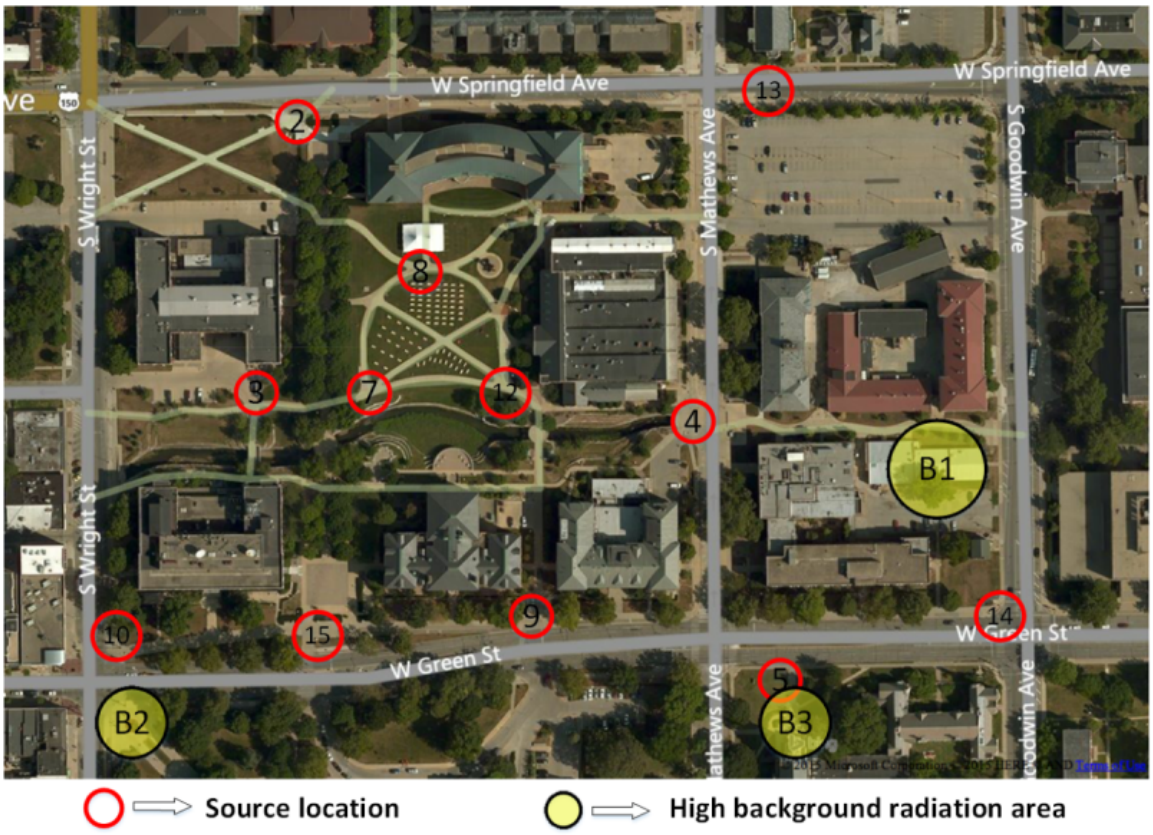

Figure 3.3: Experimental area of experiment 1 (source locations and high background radiation areas were marked with different colors)

Experiment 1 was conducted over three days (12/11/2015, 12/14/2015 and 12/15/2015). For each day, the normal background radiation data were collected first, which means that there were no manually-placed sources in the experimental area. Then, some sources were placed in the experimental area at different locations. In experiment 1, to make sure that the data were collected under different conditions, the sources should be distributed in different locations, including both grass lawn as well as road side. In addition, the placement of sources should make sure that the detectors can pass by these sources in each experiment. So, all the sources were located at pedestrian sidewalks across the experimental area (detailed locations were shown in Figure 3.3).

Each time, only one source was placed at a fixed point. Later, the source location was changed and the experiment was repeated again. So, there were five steps for each day and totally fifteen measurements for three days. The twelve source locations were marked in Figure 3.3 (location 2, 3, 4, 5 for the first day, location 7, 8, 9, 10 for the second day and location 12, 13, 14, 15 for the last day). The sources for three days kept the same during the experiment. So, there were 5 data sets for each day and totally 15 data sets for experiment 1. Note that there were three areas marked by yellow circles. These three areas included the Nuclear Radiation Laboratory (B1), the Alma Mater statue (B2) and the Wesley United Methodist Church (B3). These areas were previously observed and had much higher background radiation levels than other areas. A detailed procedures for experiment 1 is shown in Table 3.1.

Table 3.1: Experiment 1 procedures

Date	Step one (No source)	Step two	Step three	Step four	Step five
12/11/2015	Background Radiation	Source 2	Source 3	Source 4	Source 5
12/14/2015	Background Radiation	Source 7	Source 8	Source 9	Source 10
12/15/2015	Background Radiation	Source 12	Source 13	Source 14	Source 15

To cover the whole experimental area, each day in experiment 1, there were 3 operators who carried at least two detectors. The background radiation was measured first by all detectors for each day. The route for each operator was different, but each operator's route remained the same for the duration of the entire experiment and all operators walked steadily. The three routes were shown in Figure 3.4, which covered a large part of the experimental area.

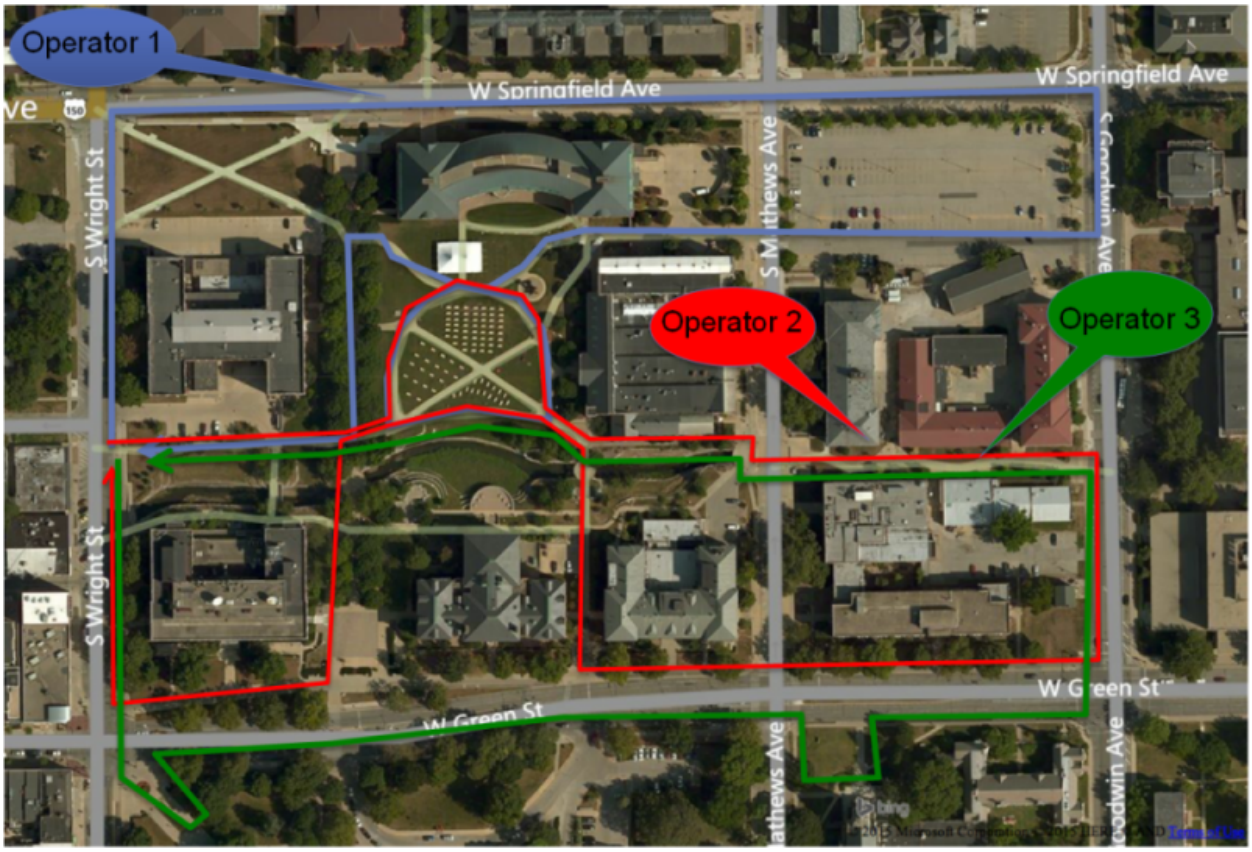

Figure 3.4: Experimental routes for three operators

3.2.2 Experiment 2

Experiment 1 was designed to study the performance of the PCA-based method on real-world data. Experiment 2, on the other hand, was designed to study the influence of integration time on the PCA-based method. It was based on experiment 1, and more details of which would be covered in chapter 4.

In experiment 1, the data were collected for every second. For 512 channels, generally, there were only 30 to 60 counts in total and most of them concentrated in the low energy region. The spectral quality was therefore not high. However, PCA decomposition and reconstruction method was based on spectral decomposition and reconstruction. These low-quality spectra would affect the system's performance (see chapter 4 for details). Since extending the integration time can improve the spectral quality, experiment 2 was designed to study the influence of the spectral quality on the PCA-based method through integrating multiple spectra.

In this experiment, to avoid the influence of high background radiation areas, the experimental area was restricted to the Bardeen Quadrangle. This area was shown in Figure 3.4. During experiment 2, there was

only one operator who carried three detectors. Similar to experiment 1, the background radiation data were collected first. Then, some sources were placed at the center of the experimental area (red circle in Figure 3.5) and the data were collected again. A detailed procedures for experiment 2 is shown in Table 3.2.

Table 3.2: Experiment 2 procedures

Experimental Date	02/06/2016
Step one	Collect data without sources
Step two	Collect data with sources present

Besides the experimental area, another important difference from experiment 1 was the walking speed. Experiment 2 was designed to study the influence of spectral quality, the spectra needed to be collected not only for one second, but also for two seconds, three seconds and so on. However, the D3S detectors only collected the data for every second. To solve this, the spectra needed to be combined manually for different integration time. To ensure that the combined spectra still reflected the radiation characteristics as mush as possible, the walking speed needed to be much lower than in experiment 1.

One thing to be noticed is that, in experiment 1 and 2, although all operators carried the same detectors and were required to walk steadily along the same path during the experiment, and the sources are the same, there were still factors that cannot be controlled, such as the changing background radiation. So, it was impossible to have the exact same conditions for each experiment. The reproducibility may be an issue for this research.

Figure 3.5: Experimental area of experiment 2 (red circle marks the location of sources)

3.3 Data Description

In this thesis, the only used information were GPS and spectra, and time was not considered. The data from different detectors were treated equally. The post-analysis rather than real-time analysis was conducted. In addition, during the experiment, we did notice that some detector didn't work properly. For example, some detectors lost power quickly and died before finishing the experiment and some detectors didn't collect the data every second. For these detectors, we didn't use the data collected by them. After analyzing the collected data, we chose the data that were collected by the detectors that worked properly during the experiment. A detailed count rate distribution of background radiation from experiment 1 and experiment 2 was shown in Table 3.3.

Table 3.3: Background radiation count rate distribution

Item	measurements	mean (cps)	std (cps)	minimum (cps)	maximum (cps)
Experiment 1	32455	35.71	9.73	8	179
Experiment 2	8995	41.14	7.81	16	71

To build the PCA model, we chose the background radiation measurement from three days. For the anomaly detection, using the PCA model, we analyzed each source location separately for each source location. Although the detectors and cell phones were pretty modern, there were still some problems with the collected data.

The first problem was the spectral quality. Generally, the spectral quality was determined by the detector itself. Although the detector was very sensitive, its small size and short collecting time affected the spectral quality. For the normal background radiation, the average count rate in the experimental area was around 36 cps for experiment 1 and 41 cps for experiment 2. For a 512 channel spectrum, this count rate implied that, only a few channels (around 7%) had records, and most of these records were concentrated on the first 100 channels. In addition, there was significant deviation in the gross count rate of background. The standard deviation of the background radiation was more than 9 cps for experiment 1 and around 8 cps for experiment 2. The range of background radiation was from 8 to 179 cps for experiment 1 (due to high background area, see Figure 3.3 for details) and 16 to 71 cps for experiment 2. These factors directly influenced the performance of PCA-based methods (see details in chapter 4).

Secondly, there were also a few problems with the GPS data, one of which was the GPS delay. The GPS information was used to determine the location of possible radioactive materials, which was important for a mobile sensor network. In this thesis, the GPS data were acquired through the cell phones. During the experiment, it was noticed that there were some delay for the GPS information, which implied that the GPS information was not updated every second. To solve the GPS delay problems, a time step interpolation method was applied. Another big problem was the GPS accuracy. As estimated, the GPS accuracy for ordinary use was around 5 meters to 10 meters [40]. In this thesis, this amount of deviation made it difficult to accurately evaluate the system's performance (see details in chapter 4).

Finally, another potential problem was that, in this thesis, no study about the relation of detector's response to different walking speed was included due to the limit of proper instruments. There was no proper instruments to accurately measure the walking speed during the experiment and the GPS information, due to its accuracy problems, could not be used to infer the walking speed. However, since during the experiment,

all operators walked steadily and there was no big change in walking speed for experiment 1 and experiment 2. So, for this thesis, the influence of walking speed should be very small. The relation between the detector's response and walking speed might be studied in the future.

To show the details of the collected data in experiment 1, a subset of the background radiation measurements from experiment 1 were plotted in Figure 3.6. The color was proportional to the count rate. In Figure 3.6, the three areas with high background radiation levels (B1, B2 and B3 in Figure 3.3) could be clearly seen. Compared with the exact path in Figure 3.4, although the path for all experiments were kept the same, the deviation of measurements was also clear in Figure 3.6, which reflected the GPS accuracy problem.

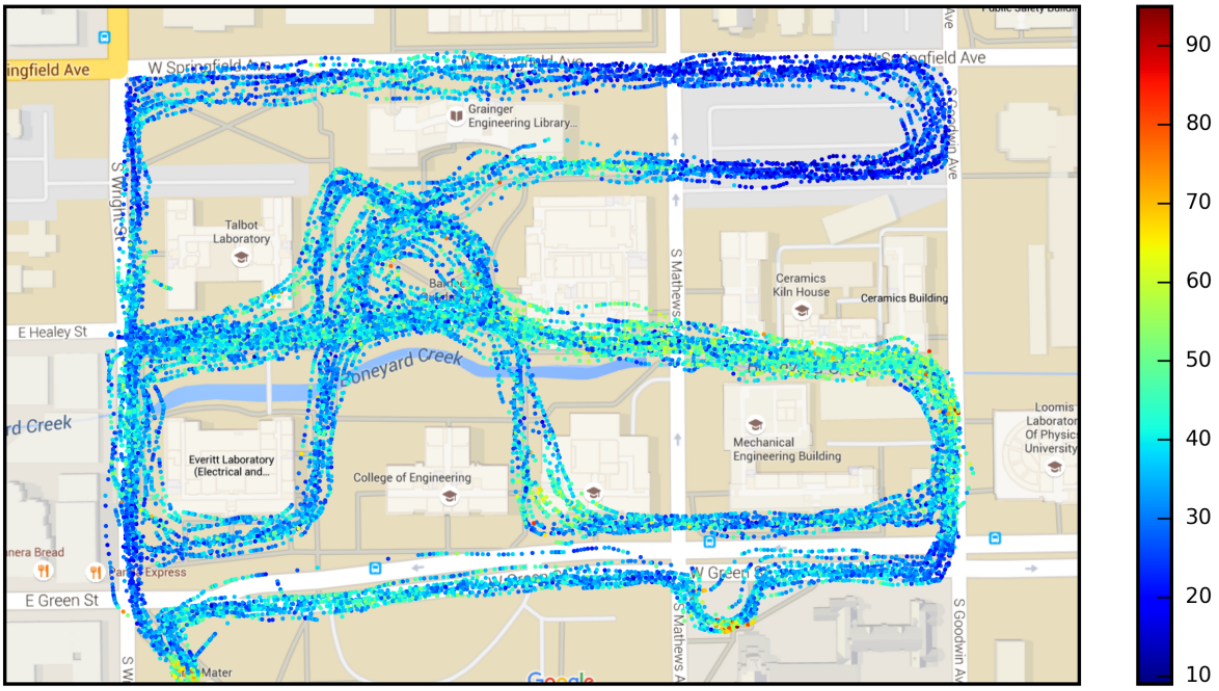

Figure 3.6: Measurements distributions for experiment 1 (data were from the background radiation measurements. Only a subset of the complete measurements were plotted. The color corresponded to the count rate (cps).)

3.4 Performance Measurement - ROC Curve

The final goal of this thesis is to test the performance of proposed method. For this purpose, the Receiver Operating Characteristic curve is used to quantitatively measure the performance of the PCA-based method.

The Receiver Operating Characteristic curve, or ROC curve [41], is a widely used graphical plot to illustrate the performance of a system. A typical ROC curve is created by plotting the true positive rate against the false positive rate at different threshold settings. In other words, it shows how many correct positive events could happen as there are more and more false positive events. For a perfect system, the true positive rate is 100%, while the false positive rate is 0. However, this kind of systems almost never happen in practice. Two sample ROC curves of different methods are shown in Figure 3.7.

For any system, a small false positive rate and a large true positive rate are always preferred. This implies that on Figure 3.7, the upper left area is always better than the lower right area. So, in figure 3.7, method 2 had an overall better performance than method 1.

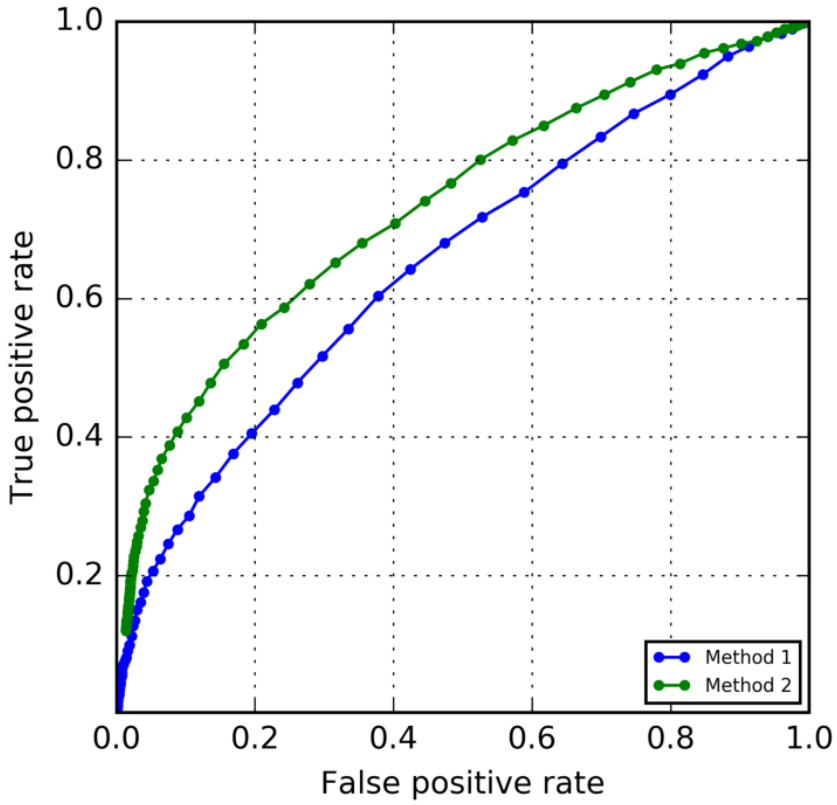

Figure 3.7: Sample ROC curves (method 1 and method 2 stand for two general sample methods)

For any radiation detection activities, there are two situations: with source or without source. The predictions from general systems also have two results: alert and non-alert. So, there are four results if the real situation and system's predictions are combined: alert when a source is present, non-alert when a source is present, alert when a source is not present and non-alert when a source is not present. The corresponding events are defined as true positive events, false negative events, false positive events and true negative events respectively. In this way, the definition of true positive rate and false positive rate are given as follows [2, 41]:

$$True\ positive\ rate\ =\ \frac{\sum True\ positive\ event}{\sum True\ positive\ event + \sum False\ negative\ event} \tag{3.2}$$

$$False\ positive\ rate\ =\ \frac{\sum False\ positive\ event}{\sum False\ positive\ event + \sum True\ negative\ event} \tag{3.3}$$

However, there is still no clear definitions for how to determine whether or not there are sources. In this thesis, since the measurements are based on mobile sensor networks, the distance is used to help determine whether or not there are sources. Suppose that the distance of one measurement from the actual source is d. With some distance threshold δ, the definition of those four events are given as follows:

$$True\ positive\ event : d \leq \delta\ and\ predicted\ to\ be\ alert \tag{3.4}$$

$$False\ negative\ event : d \leq \delta\ and\ predicted\ to\ be\ non-alert \tag{3.5}$$

$$False\ positive\ event : d > \delta\ and\ predicted\ to\ be\ alert \tag{3.6}$$

$$True\ negative\ event : d > \delta\ and\ predicted\ to\ be\ non-alert \tag{3.7}$$

Considering the GPS accuracy issue, the distance threshold δ is finally chosen to be 10m.

With the ROC curve, the performance of different methods could be compared directly, such as method 1 and method 2 in Figure 3.7. However, when there are more than three methods, plotting all the ROC curves in one figure makes it hard to distinguish with each other. In this case, the concept of the area under the ROC curve (AUC or AUROC) is a good choice. AUC referes to the area that is under the ROC curve [42]. AUC summarizes the ROC curve into a single number, which measures the overall performance of one system. So, for different testing systems, a system with a larger AUC is thought to have a better overall performance than the other systems with a smaller AUC. In chapter 4, both ROC curve and AUC are used to compare the different settings.

Chapter 4

Results

In chapter 3, the detector system and two experiments designed to test the performance of the proposed method were described. In this chapter, at first, PCA decomposition methods were applied to the collected radiation data and a series of principal components were obtained. Then, these principal components were used to reconstruct the spectra. Finally, the performance of the proposed PCA-based method was quantitatively measured through the ROC curve and AUC, and some explanations were given based on detailed spectral analysis.

4.1 System Performance Analysis

4.1.1 PCA Decomposition

The standard PCA decomposition method was described in section 2.2, which was easy to understand and apply. In fact, some programming languages, like Matlab and Python, have already included PCA decomposition methods as built-in functions or external packages. In this thesis, the Python scikit-learn [43] package was used to conduct PCA decomposition.

The PCA decomposition was conducted based on the background radiation data. For experiment 1, this meant the measured background radiation data in three days (step 1 in Table 3.1). For experiment 2, this meant the first measurement where there was no manually placed sources. After PCA decomposition, the average value for each channel was obtained, which corresponded to the average background radiation spectrum. Then, a series of principal components were calculated. The principal components also had 512 dimensions. Like the original spectra, only approximately the first 100 dimensions had non-zero values. To see this process clearly, the average background radiation spectrum and the first seven principal components calculated through background radiation data from experiment 1 were plotted in Figure 4.1. The first figure in Figure 4.2 corresponded to the average background radiation, and the summation, which was the average background radiation count rate, was around 36 cps.

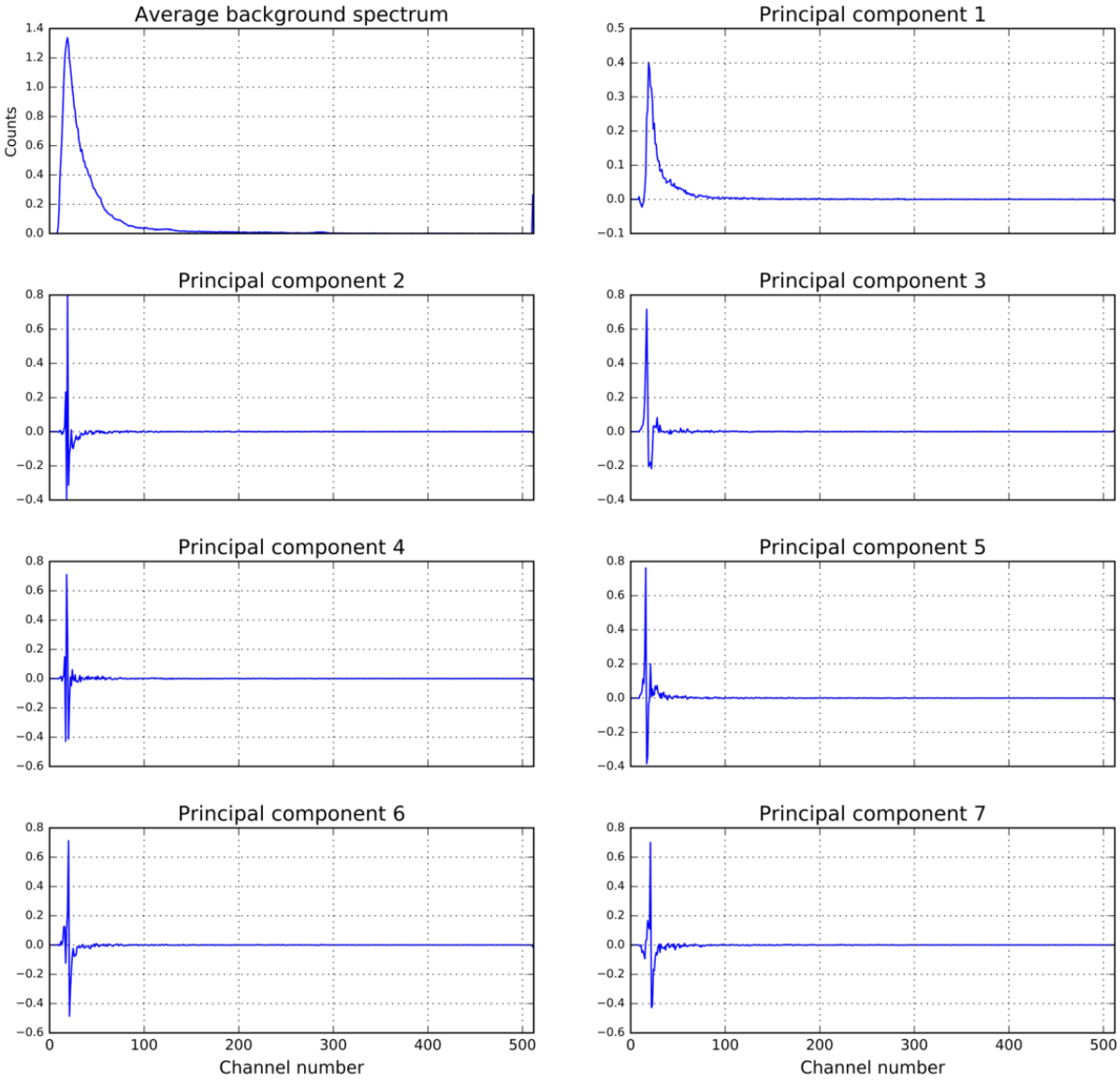

Figure 4.1: PCA decomposition illustration (including average background radiation spectrum and the first seven principal components. The background radiation data from experiment 1 are used.)

The principal components had been sorted according to the corresponding variances, but from Figure 4.1, the exact distribution of the variances was not clear. To see the relative importance of different principal components, the percentage of explained variance of each principal component were calculated and plotted in Figure 4.2.

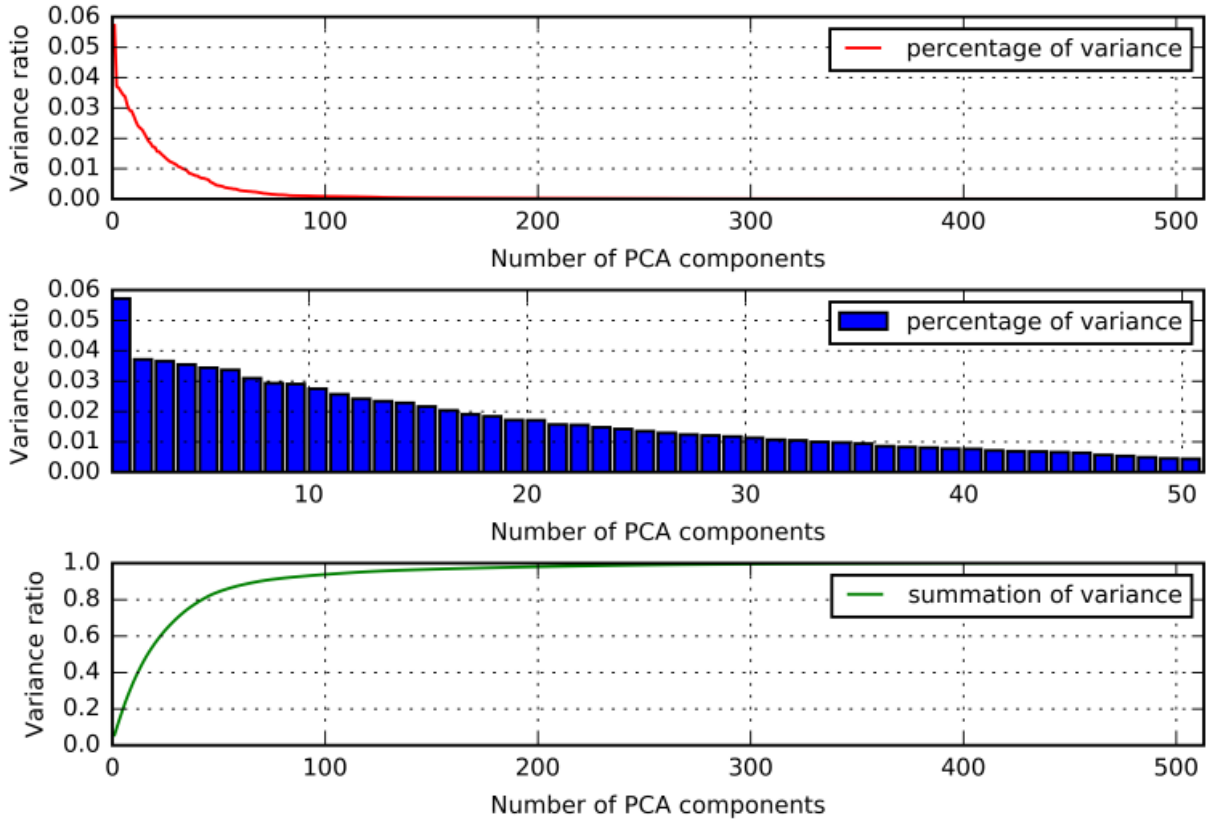

Figure 4.2: Illustration of explained variance ratio (the first figure plotted the variance percentage for all principal components, the second figure plotted the variance percentage for the first 50 principal components only, and the third figure plotted the cumulative variance percentage for different principal components)

As expected, after PCA decomposition, the first several principal components contained most of the information. This was very clear in the first figure of Figure 4.2. The explained variance was close to zero after the first 100 principal components. In the second figure, only the explained variance for the first 50 principal components was plotted to show the distribution details. The first principal component explained 5.8% of all the variance. Since the variance was thought as a measurement of the information, the first principal component was thus thought to contain 5.8% of all information. From the second principal component, the explained variance changed very smoothly. In the third figure, the cumulative percentage of different number of principal components was plotted. The first 100 principal components contained around 90% of all information for background radiation data.

4.1.2 PCA Reconstruction

After PCA decomposition, the next job was to reconstruct the unknown spectra using the obtained principal components. How to determine the number of principal components to be used was a critical problem.

Instead of choosing different numbers of principal components directly, the number of principal components to be used was determined according to the information that was to keep. According to the cumulative variances, the percentage of information to keep was first determined. Then, the number of principal components to be used was determined. For example, in Figure 4.3, 90% and 50% of the total information were chosen to reconstruct the radiation spectra collected in Experiment 1 (the data were collected when sources were placed at location 2 in Figure 3.3), which corresponded to first 67 and first 16 principal components. Then, the count rate of original spectra (blue points) and reconstructed spectra (green points) were plotted respectively.

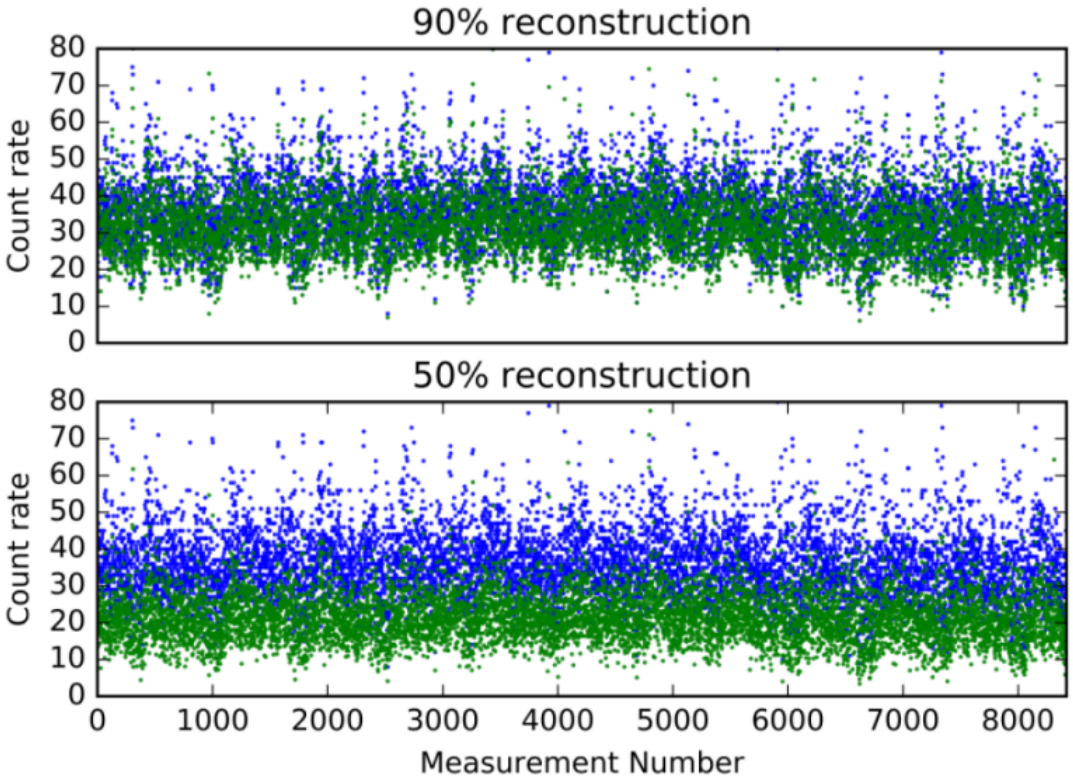

Figure 4.3: Radiation spectra reconstruction (90% and 50% of the information was used. The blue points was the count rate of original spectra, and the green points was the count rate of reconstructed spectra. A subset of radiation data with sources placed at location 2 in experiment 1 were plotted.)

In Figure 4.3, the horizontal axis means the number of measurements. More than 8000 spectra were

reconstructed. All principal components were calculated based on normal background radiation spectra collected in experiment 1. Figure 4.3 graphically showed the influence of different number of principal components on reconstruction. With less principal components, for example, using 50% information to reconstruct the spectra, the difference between original spectra and reconstructed spectra was much clear than using 50% information to reconstruct the spectra, which corresponded to the analysis in Figure 4.4.

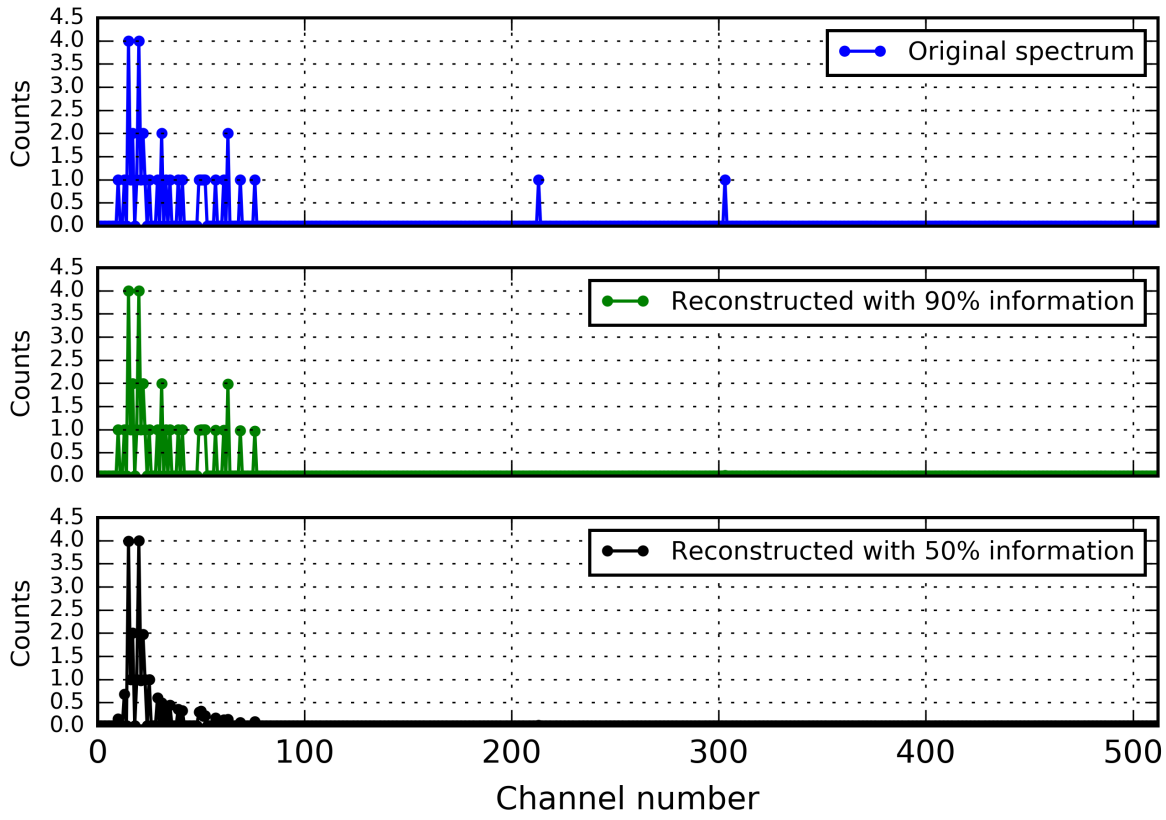

Figure 4.4: Sample spectrum reconstruction comparison (90% and 50% of the information was used to reconstruct the spectrum. The original spectrum, the spectrum reconstructed using 90% and 50% of the information were plotted respectively)

In Figure 4.4, a sample spectrum from normal background radiation was chosen. Using 90% and 50% information, the reconstructed spectra were plotted respectively. Using 90% information, the reconstructed spectra and original spectra were similar. They didn't have much difference. When the spectrum was reconstructed using only 50% information, the difference between the reconstructed spectrum and the original spectrum was clear.

In addition, note the fact that when there were sources present, the collected spectra showed some

difference from the normal background radiation, such as some peaks in the higher energy region (see Figure 2.2 in chapter 2 for details). In this way, the count rate difference between the original spectra and the reconstructed spectra could be used as an indicator to distinguish the spectra with unknown sources from the spectra with normal background radiation level. With an appropriate threshold, the measurements whose count rate difference was above the threshold were thought to be alert measurements, while the measurements whose count rate difference was below the threshold were thought to be non-alert measurements. To see this, 50% of all information (first 16 principal components) was used to reconstruct the experimental data acquired from experiment 1. With a small threshold as well as a large threshold, the predicted alert points (green points) and non-alert points (yellow points) were plotted on a 2D map. In addition, the manually placed radioactive sources (red circle) were also plotted on the same map. The result was shown in Figure 4.5.

In Figure 4.5, with a small threshold, there was a large chance that all alert measurements were detected, which implied the true positive rate was higher. However, a small threshold also increased the chance that a normal background radiation spectrum being thought to contain source information, which increased the false positive rate. On the other hand, with a large threshold, the false positive rate could be decreased, but the true positive rate was also decreased. This was clearly shown in Figure 4.5. In Figure 4.5, with a small threshold, the points that were around the sources were predicted as alert measurements. On other areas where the measurements were far away from any source, however, there were several measurements predicted to be alert measurements, which means that the false positive rate was high. Instead, with a large threshold, the number of false positive events was much less than the situation with a small threshold. But with a large threshold, several measurements that were around the sources couldn't be correctly predicted, which decreased the true positive rate.

Another interesting phenomenon was that, with both a large threshold and a small threshold, on the areas (B1, B2 and B3 in Figure 3.2) where the background radiation level was higher, several measurements were predicted to be alert measurements.

In Figure 4.5, the thresholds for each figure were chosen manually. For actual applications, thresholds should be chosen based on ROC curve analysis. According to different requirements, the allowed false positive rate and true positive rate were determined and the corresponding thresholds were also determined.

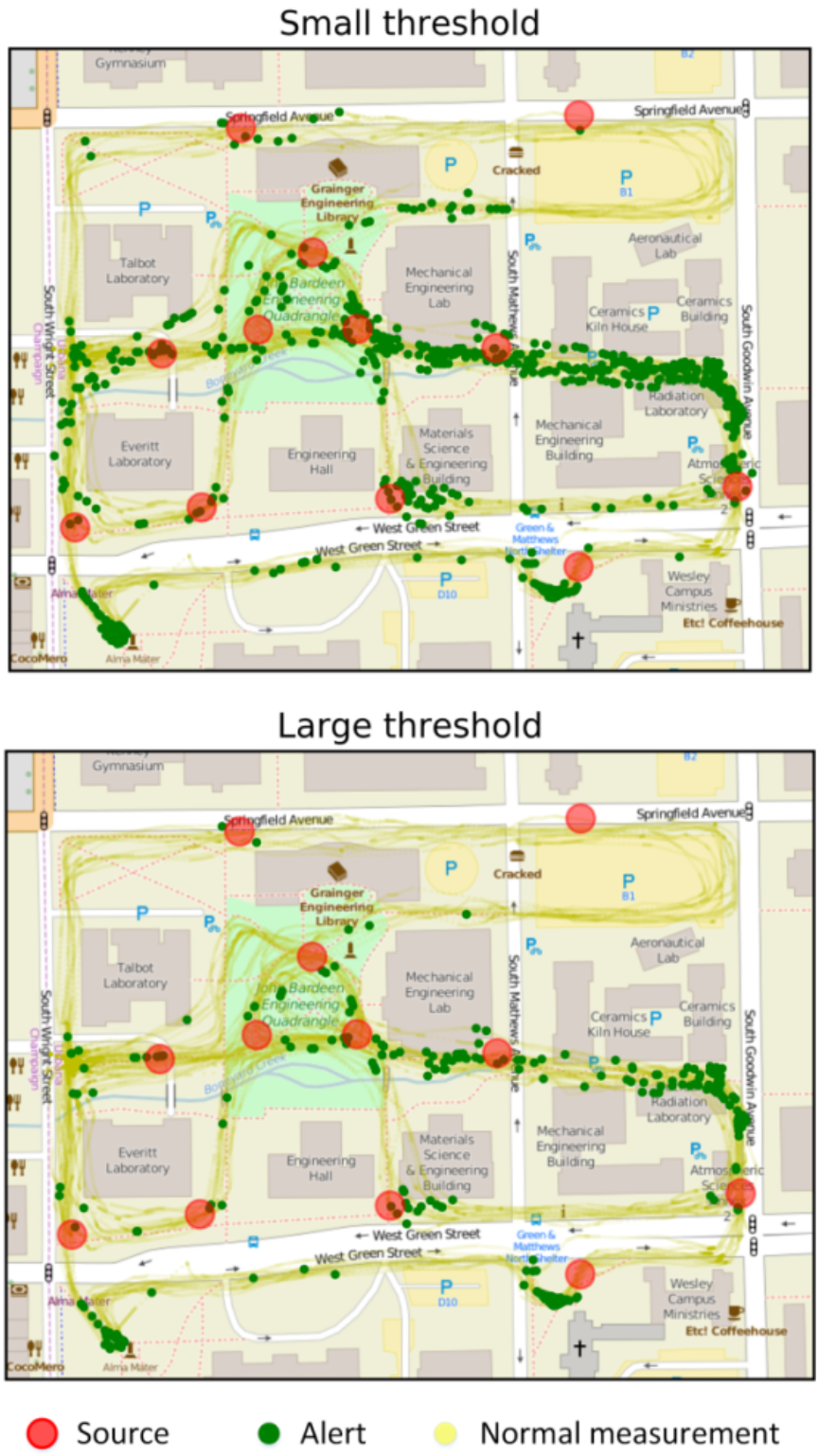

Figure 4.5: System performance test on experiment 1 (using 50% information (first 16 principal components) to reconstruct the spectra. Source location, alert and normal measurements were shown with different colors. The corresponding thresholds were 24 cps and 27 cps for each figure individually.)

From the above analysis, the influence of the number of principal components and the threshold was clear. In order to increase the true positive rate while decreasing the false positive rate, two parameters needed to be tuned: the number of principal components and the magnitude of threshold. With the ROC curve, their influence was seen clearly.

In Figure 4.6, 90%, 70% and 50% of all information were chosen to reconstruct the spectra collected in experiment 1, which corresponds to first 67, 29 and 16 principal components. The true positive rate and false positive rate were calculated according to the definition in section 3.4. As a comparison, the traditional k-sigma method was also used to calculate the true positive rate and false positive rate. The corresponding ROC curve was plotted in the same figure.

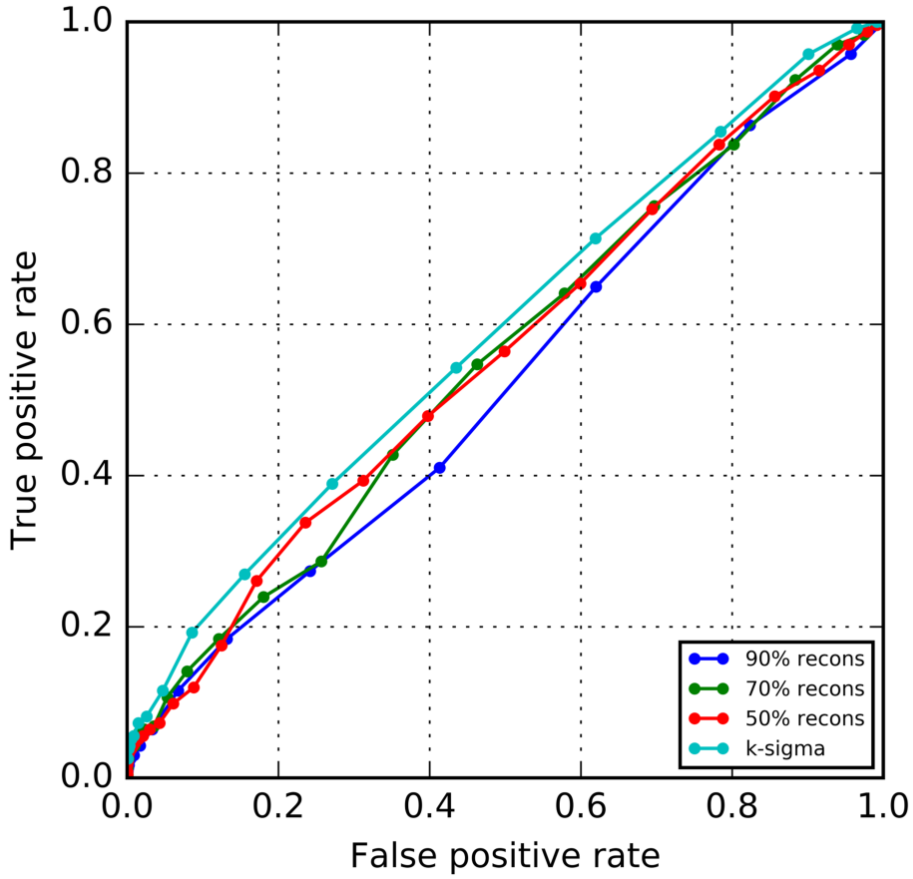

Figure 4.6: ROC curves for experiment 1 (all the results were calculated based on 1 s spectra collected by D3S detectors in experiment 1)

In Figure 4.6, as less principal components were used to reconstruct the spectra, the system's overall performance was improved. This proved the feasibility of proposed PCA-based decomposition and recon-

struction method.

The results in Figure 4.5 and Figure 4.6 were a little worse than expected, especially compared with the result shown in Figure 2.2. The influence of detector's sensitivity could explain this. As expected, with a better detector, for example, in Figure 2.2, the result should be very good. However, more sensitive detector meant larger size and less mobility. Currently, the small D3S detectors were the only possible choice. Other detectors, such as the NaI detector used in Figure 2.2, cannot be used as the mobile sensors. More verification work will be conducted in the future.

In Figure 4.6, among all three ROC curves, even the best one, which was obtained by using 50% of the information to reconstruct the spectra, was below the ROC curve of traditional k-sigma method. In next section, some explanations were given to explain this phenomenon.

4.2 Explanation

Figure 4.6 showed that the performance of the proposed PCA-based method was worse than the traditional k-sigma method. There were several reasons that could explain this phenomenon.

The first reason was related to the detector systems. It was known that there were slight detector-to-detector variations in total efficiency. Even adjusted algorithmically, this difference always existed between different detectors, which influenced the system's performance. In addition, cell phones, which were used to determine the exact locations in experiment, had different GPS accuracies. Since the distance was used to calculate the true positive rate and false positive rate, GPS accuracy also influenced the system's performance. In this thesis, GPS information was used to measure the proposed method's performance. However, for the real scenario where the exact locations of actual sources were unknown, GPS information was used to find the possible locations where there might be sources.

Secondly, in this thesis, all the measurements that were within 10 m of real sources were thought to contain source information. In fact, only part of them contained the source information. This assumption decreased the true positive rate.

Thirdly, there were three areas (B1, B2 and B3 in Figure 3.3) that had much higher background radiation level. After PCA analysis, some measurements in these areas were thought to be alerts. However, this wasn't considered in the analysis because the boundaries of the areas were hard to accurately determine. This increased the false positive rate.

The last reason, which was almost the most important reason, was the spectral quality. The proposed method was based on spectral analysis, so its performance was directly determined by spectral quality. To

see this, two sample measurements were chosen: one had a low count rate (35 counts per second) and was far away from the actual source (more than 20 m), and the other one had a high count rate (88 counts per second) and was close to the same source (less than 5 m). The original spectra, reconstructed spectra and their difference were plotted separately in Figure 4.7.

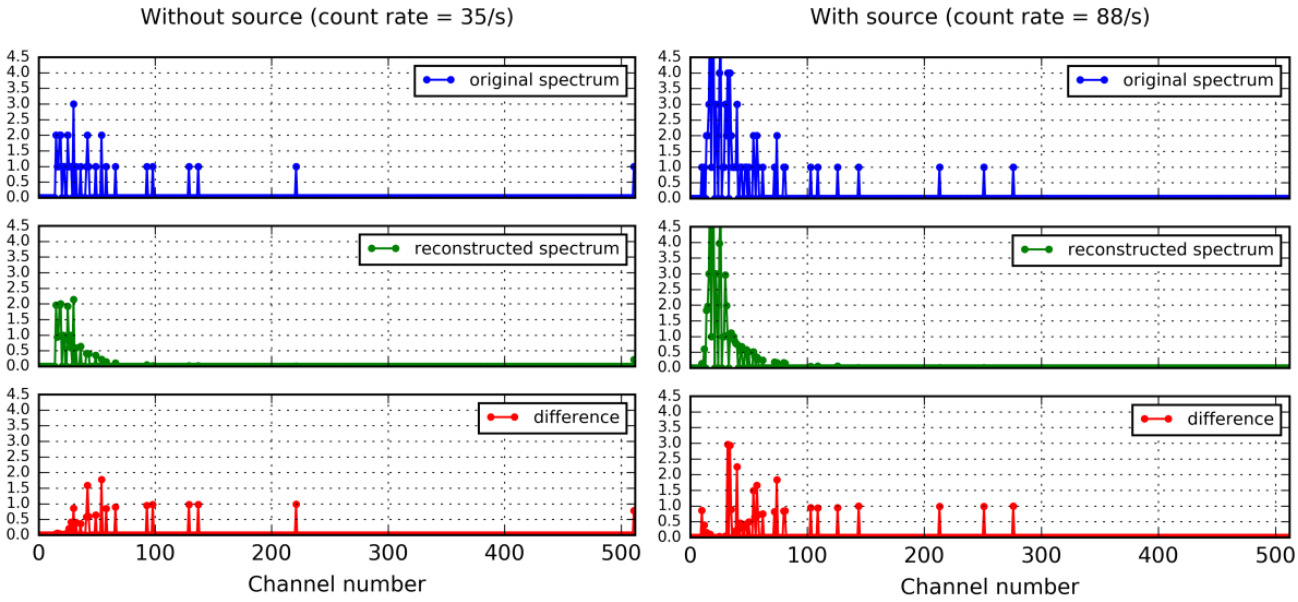

Figure 4.7: Spectrum comparison 1

In Figure 4.7, the red spectra, which were calculated by subtracting the reconstructed spectra from the original spectra, were thought to mainly contain the source information. Their count rates were used to determine whether or not there were unknown sources. After PCA decomposition and reconstruction, the bottom right spectrum in Figure 4.7 had a higher count rate than the bottom left spectrum. Choosing appropriate threshold, these two spectra could be distinguished easily. In this case, the PCA-based method could make right decisions.

However, when the measurements were close to the source but had a medium count rate, the PCA-based method might not work. In Figure 4.8, two measurements were plotted: one measurement was far away (more than 20 m) from the actual source and had a low count rate (30 counts per second), and the other one was close (less than 5 m) to the actual source but had a medium count rate (47 counts per second).

In Figure 4.8, although the measurement that was close to source had a higher count rate than the normal background radiation (30 counts per second), after PCA decomposition and reconstruction, its source spectrum (bottom right spectrum) is similar to the spectrum from normal background (bottom left spectrum). The threshold that worked for the situation in Figure 4.7 didn't work for Figure 4.8. In this

case, the PCA-based method couldn't make right decisions.

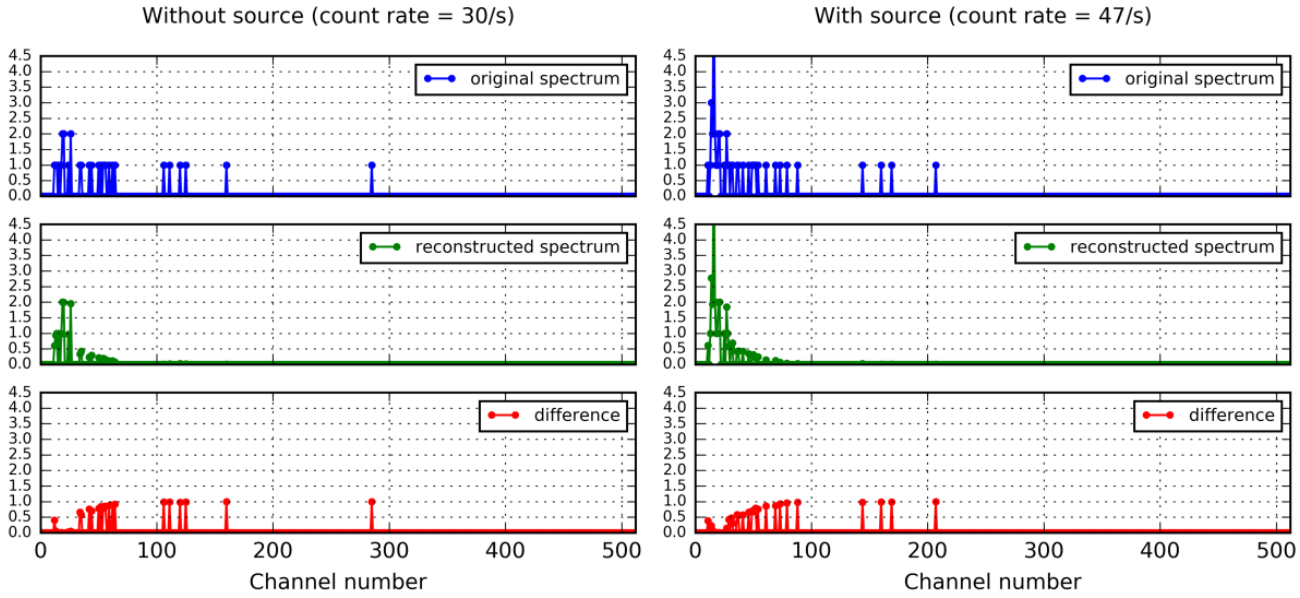

Figure 4.8: Spectrum comparison 2

From Figure 4.7 and Figure 4.8, when the measurements that were close to sources only had a medium count rate, the PCA-based method couldn't correctly distinguish them from normal background radiation. Comparing with the theoretical analysis in chapter 2, it was easy to conclude that this phenomenon was related to the spectral quality. With a small detector and only a 1 second collection time, the peak region, which reflected the characteristics of unknown sources, couldn't be clearly identified. This was why spectral quality influenced the performance of the PCA-based method.

The above four reasons could help with understanding the result shown in Figure 4.6. The next section focused on the influence of spectral quality on the PCA-based method.

4.3 Performance Analysis

Since spectral quality greatly affected the performance of the PCA-based method, to obtain a better performance, one simple idea was to improve the spectral quality. Based on experiment 1, experiment 2 was designed to study the influence of spectral quality on the proposed method. In experiment 2, the experimental area was restricted to the Bardeen Quadrangle only (shown in Figure 3.5), and the high background radiation areas (B1, B2 and B3 in Figure 3.3) were excluded. To improve the spectral quality, one choice was to use more sensitive detectors, which was not realistic for this thesis. Another choice was to extend the

collection time from 1 second to multiple seconds. However, the detector only collected spectra for every second, so the spectra needed to be combined manually to obtain the spectra for more than 1 second. To make sure that the combined spectra still reflected the characteristics of any sources, the walking speed was decreased and the operator walked in a straight line as much as possible. Then, the spectra were combined according to different integration time. Through PCA decomposition and reconstruction using 60% of the information, the true positive rate and false positive rate were calculated according to the definition in chapter 3. Finally, the ROC curves for different integration time were plotted respectively in Figure 4.9. Figure 4.9 proved that improving the spectral quality (through increasing the integration time) could improve the performance of PCA-based method.

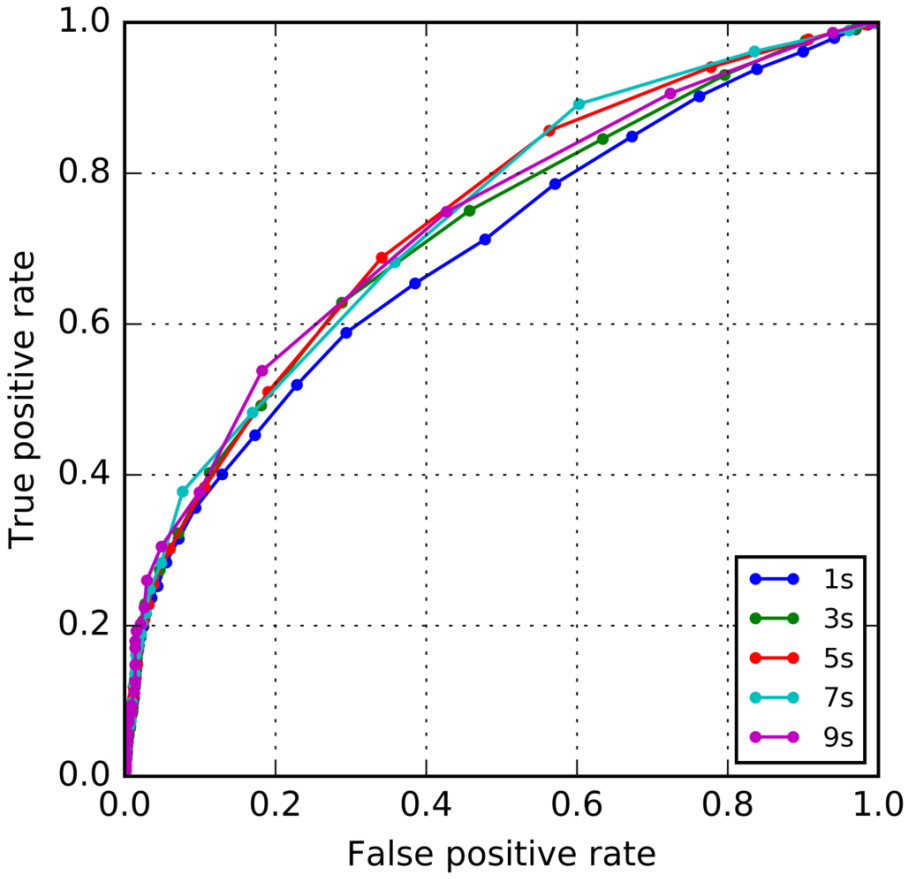

Figure 4.9: ROC curves for experiment 2 with different integration time (using 60% of the information for spectrum reconstruction)

The ROC curves in experiment 2 performed much better than those in experiment 1. This was because

that, in experiment 2, the high background radiation areas (B1, B2 and B3 in Figure 3.3) were not included. According to the analysis in section 4.2, the false positive rate was therefore decreased, which made the overall performance of the ROC curves in experiment 2 to be better than the ROC curves obtained in experiment 1 (see Figure 4.6 for details).

Increasing the integration time from 1 s to 10 s, the system's overall performance improved. However, this improvement was not very clear since the five ROC curves entangle with each other. According to section 3.4, the area under the ROC curve, or AUC, can be used to see the difference between the ROC curves. In Figure 4.10, the change of AUC for different integration time was plotted.

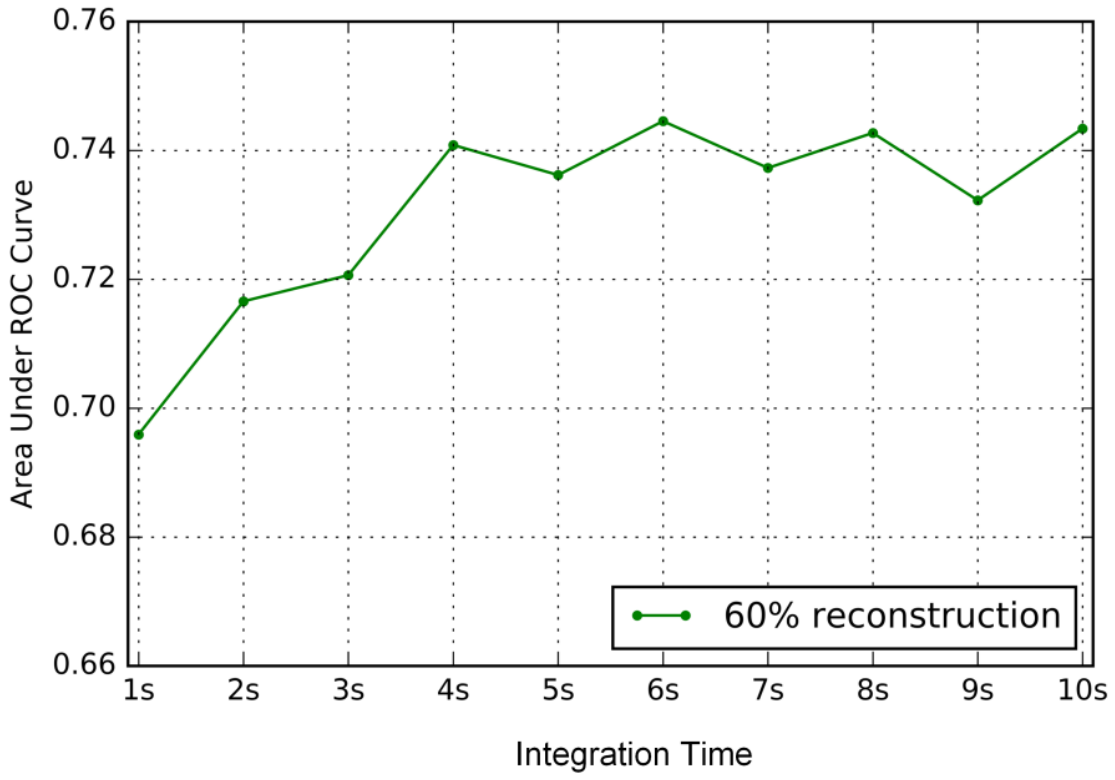

Figure 4.10: AUC for different integration time (using 60% information for spectrum reconstruction)

As the integration time increased from 1 s to 10 s, there was an increasing trend of AUC. In fact, the increase trend only continued from 1 s to 4 s. After 4 s, the AUC was fluctuating around 0.74. This phenomenon could be explained as follows:

1, From 1 s to 4 s, through the increment of integration time, the spectral quality was improved and the combined spectra could still reflect the characteristics of unknown sources. So, the system's

performance improved.

2, After 4 s, through the increment of integration time, the spectral quality was improved. However, after a large integration time, the detector has already been far from the source. The combined spectra will contain more and more background information rather the source information. So, the system's performance couldn't be further improved. What's more, the system's performance might be even worse if too many spectra were combined.

The above analysis proved the preliminary hypothesis that the spectral quality affected the proposed method's performance. This limited the application of the PCA-based method. But when the spectral quality got improved, according to the theoretical analysis, the performance of PCA-based method should improve.

Chapter 5

Conclusions

5.1 Contributions

In this thesis, the impact of a PCA-based algorithm for radiation detection using mobile sensor networks were studied. This was done as follows:

First of all, the characteristics of mobile sensor network were analyzed and it was proven to be a good choice for radiation detection in large areas for moving or stationary sources. Then, with the D3S detectors and cell phones, a small mobile sensor network was successfully established.

Secondly, based on the idea of estimating the background radiation, the PCA decomposition and reconstruction method was proposed. Its performance on mobile sensor networks was then quantitatively analyzed through experiment 1.

Finally, based on the observed phenomenon from experiment 1, experiment 2 was designed and the impact of spectral quality on the PCA-based method's performance was studied, which provided a good reference for future work in related areas.

Although the PCA-based method currently performed worse than k-sigma method, further studies showed that its performance could be improved by improving the spectral quality. The future work will be focused on improving spectral quality through algorithms as well as developing new methods to solve similar issues.

5.2 Future Work

Detecting and localizing possible sources using mobile sensor networks is very challenging. There are a lot of problems to be solved in the future. Some potential directions for future work include:

1. Improve spectral quality. Using signal processing techniques or other methods to improve the spectral quality, such as smoothing or fitting the low quality spectra. In this way, the performance of PCA-based method and other spectrum based analysis methods can be improved.

2. Couple different analysis methods together. Using spectral information only is not enough, especially

when the spectral quality is low. Combining spectral analysis methods with other methods like MLE or Bayesian methods makes it possible to draw more robust conclusions.

3. Clustering techniques. Try appropriate clustering methods from machine learning, such as density-based spatial clustering of applications with noise (DBSCAN) methods to correctly classify normal background radiation spectra and the spectra with unknown radioactive materials.

4. Anomaly detection. Try anomaly detection techniques, especially semi-supervised anomaly detection techniques, to identify the spectra associated with unknown radioactive materials.

References

[1] United Nations. Scientific Committee on the Effects of Atomic Radiation. *Sources and effects of ionizing radiation: sources*, volume 1. United Nations Publications, 2000.

[2] G. F. Knoll. *Radiation detection and measurement*. John Wiley & Sons, 2010.

[3] J. H. Ely, R. T. Kouzes, B. D. Geelhood, J. E. Schweppe, and R. A. Warner. Discrimination of naturally occurring radioactive material in plastic scintillator material. *Nuclear Science, IEEE Transactions on*, 51(4):1672–1676, 2004.

[4] N. Salikhov and O. Kryakunova. An increase of the soft gamma-ray background by precipitations. In *International Cosmic Ray Conference*, volume 11, page 367, 2011.

[5] R. J. Livesay, C. S. Blessinger, T. F. Guzzardo, and P. A. Hausladen. Rain-induced increase in background radiation detected by Radiation Portal Monitors. *Journal of environmental radioactivity*, 137:137–141, 2014.

[6] S. Minato. Analysis of time variations in natural background gamma radiation flux density. *Journal of Nuclear Science and Technology*, 17(6):461–469, 1980.

[7] Y. T. Yang, B. Fishbain, D. S. Hochbaum, E. B. Norman, and E. Swanberg. The supervised normalized cut method for detecting, classifying, and identifying special nuclear materials. *INFORMS Journal on Computing*, 26(1):45–58, 2013.

[8] E. B. Norman, S. G. Prussin, R. Larimer, H. Shugart, Ed. Browne, A. R. Smith, R. J. McDonald, H. Nitsche, P. Gupta, M. I. Frank, et al. Signatures of fissile materials: high-energy γ rays following fission. *Nuclear Instruments and Methods in Physics Research Section A: Accelerators, Spectrometers, Detectors and Associated Equipment*, 521(2):608–610, 2004.

[9] W. Bertozzi and R. J. Ledoux. Nuclear resonance fluorescence imaging in non-intrusive cargo inspection. *Nuclear Instruments and Methods in Physics Research Section B: Beam Interactions with Materials and Atoms*, 241(1):820–825, 2005.

[10] K. M. Chandy, J. Bunn, and A. Liu. Models and algorithms for radiation detection. In *Modeling and Simulation Workshop for Homeland Security*, pages 1–6, 2010.

[11] A. H. Liu. *Simulation and implementation of distributed sensor network for radiation detection*. PhD thesis, California Institute of Technology, 2010.

[12] A. H. Liu, J. J. Bunn, and K. M. Chandy. Sensor networks for the detection and tracking of radiation and other threats in cities. In *Information Processing in Sensor Networks (IPSN), 2011 10th International Conference on*, pages 1–12. IEEE, 2011.

[13] M. R. Morelande and B. Ristic. Radiological source detection and localisation using Bayesian techniques. *Signal Processing, IEEE Transactions on*, 57(11):4220–4231, 2009.

[14] M. Chandy, C. Pilotto, and R. McLean. Networked sensing systems for detecting people carrying radioactive material. In *Networked Sensing Systems, 2008. INSS 2008. 5th International Conference on*, pages 148–155. IEEE, 2008.

[15] S. M. Brennan, A. M. Mielke, and D. C. Torney. Radioactive source detection by sensor networks. *Nuclear Science, IEEE Transactions on*, 52(3):813–819, 2005.

[16] R. J. Nemzek, J. S. Dreicer, D. C. Torney, and T. T. Warnock. Distributed sensor networks for detection of mobile radioactive sources. *Nuclear Science, IEEE Transactions on*, 51(4):1693–1700, 2004.

[17] M. Morelande, B. Ristic, and A. Gunatilaka. Detection and parameter estimation of multiple radioactive sources. In *Information Fusion, 2007 10th International Conference on*, pages 1–7. IEEE, 2007.

[18] K. D. Jarman, L. E. Smith, D. K. Carlson, and D. N. Anderson. Sequential probability ratio test for long-term radiation monitoring. In *Nuclear Science Symposium Conference Record, 2003 IEEE*, volume 2, pages 1458–1462. IEEE, 2003.

[19] J. Chin, N. Rao, D. Yau, M. Shankar, Y. Yang, J. C. Hou, S. Srivathsan, and S. Iyengar. Identification of low-level point radioactive sources using a sensor network. *ACM Transactions on Sensor Networks (TOSN)*, 7(3):21, 2010.

[20] N. Rao, J. Chin, D. Yau, and C. Ma. Localization leads to improved distributed detection under non-smooth distributions. In *Information Fusion (FUSION), 2010 13th Conference on*, pages 1–8. IEEE, 2010.

[21] N. Rao, M. Shankar, J. Chin, D. Yau, C. Ma, Y. Yang, J. C. Hou, X. Xu, and S. Sahni. Localization under random measurements with application to radiation sources. In *Information Fusion, 2008 11th International Conference on*, pages 1–8. IEEE, 2008.

[22] J. W. Howse, L. O. Ticknor, and K. R. Muske. Least squares estimation techniques for position tracking of radioactive sources. *Automatica*, 37(11):1727–1737, 2001.

[23] J. Chin, D. Yau, N. Rao, Y. Yang, C. Ma, and M. Shankar. Accurate localization of low-level radioactive source under noise and measurement errors. In *Proceedings of the 6th ACM conference on Embedded network sensor systems*, pages 183–196. ACM, 2008.

[24] S. M. Brennan, A. M. Mielke, D. C. Torney, and A. B. MacCabe. Radiation detection with distributed sensor networks. *Computer*, 37(8):57–59, 2004.

[25] D. S. Hochbaum. The multi-sensor nuclear threat detection problem. In *Operations Research and Cyber-Infrastructure*, pages 389–399. Springer, 2009.

[26] D. S. Hochbaum and B. Fishbain. Nuclear threat detection with mobile distributed sensor networks. *Annals of Operations Research*, 187(1):45–63, 2011.

[27] P. Tandon, P. Huggins, A. Dubrawski, S. Labov, and K. Nelson. Detection of radioactive sources using Bayesian aggregation of data from mobile spectrometers.

[28] M. Alamaniotis, J. Mattingly, and L. H. Tsoukalas. Kernel-based machine learning for background estimation of NaI low-count gamma-ray spectra. *Nuclear Science, IEEE Transactions on*, 60(3):2209–2221, 2013.

[29] J. M. Kirkpatrick and B. M. Young. Poisson statistical methods for the analysis of low-count gamma spectra. *Nuclear Science, IEEE Transactions on*, 56(3):1278–1282, 2009.

[30] R. Fischer, K. M. Hanson, V. Dose, and W. Von Der Linden. Background estimation in experimental spectra. *Physical Review E*, 61(2):1152, 2000.

[31] M. Morháč, J. Kliman, V. Matoušek, M. Veselskỳ, and I. Turzo. Background elimination methods for multidimensional coincidence γ-ray spectra. *Nuclear Instruments and Methods in Physics Research Section A: Accelerators, Spectrometers, Detectors and Associated Equipment*, 401(1):113–132, 1997.

[32] M. Morháč. An algorithm for determination of peak regions and baseline elimination in spectroscopic data. *Nuclear Instruments and Methods in Physics Research Section A: Accelerators, Spectrometers, Detectors and Associated Equipment*, 600(2):478–487, 2009.

[33] M. H. Zhu, L. G. Liu, Y. S. Cheng, T. K. Dong, Z. You, and A. A. Xu. Iterative estimation of the background in noisy spectroscopic data. *Nuclear Instruments and Methods in Physics Research Section A: Accelerators, Spectrometers, Detectors and Associated Equipment*, 602(2):597–599, 2009.

[34] C. Fraschini and F. Chaillan. Background spectrum estimation via robust Kalman filtering. In *New Trends for Environmental Monitoring Using Passive Systems, 2008*, pages 1–6. IEEE, 2008.

[35] L. V. East, R. L. Phillips, and A. R. Strong. A fresh approach to NaI scintillation detector spectrum analysis. *Nuclear Instruments and Methods in Physics Research*, 193(1-2):147–155, 1982.

[36] M. S. Mitra and P. K. Sarkar. Monte Carlo simulations to estimate the background spectrum in a shielded NaI (Tl) γ-spectrometric system. *Applied radiation and isotopes*, 63(4):415–422, 2005.

[37] S. Theodoridis and K. Koutroumbas. *Pattern Recognition*. Elsevier Science, 2008.

[38] M. B. Christopher. Pattern recognition and machine learning. *Company New York*, 16(4):049901, 2006.

[39] R. C. Runkle, M. F. Tardiff, K. K. Anderson, D. K. Carlson, and L. E. Smith. Analysis of spectroscopic radiation portal monitor data using principal components analysis. *Nuclear Science, IEEE Transactions on*, 53(3):1418–1423, 2006.

[40] M. G. Wing, A. Eklund, and L. D. Kellogg. Consumer-grade global positioning system (GPS) accuracy and reliability. *Journal of forestry*, 103(4):169–173, 2005.

[41] C. E. Metz. Basic principles of ROC analysis. In *Seminars in nuclear medicine*, volume 8, pages 283–298. Elsevier, 1978.

[42] J. A. Hanley and B. J. McNeil. The meaning and use of the area under a receiver operating characteristic (ROC) curve. *Radiology*, 143(1):29–36, 1982.

[43] F. Pedregosa, G. Varoquaux, A. Gramfort, V. Michel, B. Thirion, O. Grisel, M. Blondel, P. Prettenhofer, R. Weiss, V. Dubourg, J. Vanderplas, A. Passos, D. Cournapeau, M. Brucher, M. Perrot, and E. Duchesnay. Scikit-learn: Machine learning in Python. *Journal of Machine Learning Research*, 12:2825–2830, 2011.